Active Engine Noise Cancellation Using Vibro-Acoustic Modeling

by

Matthew J. Wickman

A thesis in partial fulfillment
of the requirements for the degree of
Master of Science in Engineering
(Mechanical Engineering)
in the University of Michigan-Dearborn
2023

Master's Thesis Committee:

Emeritus Professor John Cherng, Co-Chair
Assistant Professor Youngki Kim, Co-Chair
Associate Professor Linda Zhu
Lecturer Taner Onsay

Dedication

To Alyssa and Ada, without whom I would never have been able to persevere through the challenges of the last few years of my education. You both have given me endless love and plenty of patience. You've given me the strength to do difficult things in hard times. I will always be there to repay the favor.

Acknowledgements

I wish to express my deep appreciation to my thesis advisors and committee co-chairs, Dr. John Cherng and Dr. Youngki Kim. Their guidance, reassurance and technical knowledge has been critical in the success of this project. Their genuine kindness and professionalism has made organizing and planning in odd times as frictionless as possible. As I continue in my life and my career, I hope that both of you are reminded often of how you enable your students (past and present) to succeed as you have done for me.

Furthermore, to Dr. Zhu, Dr. Onsay and Dr. Han, I owe my thanks for the time and commitment you have each given me to ensure that this research was answering real and valuable questions in our world by challenging assumptions, asking great questions and providing tips along the way. I am so happy that we have been able to collaborate with each other and I would be elated to find our paths crossing again in the future.

To Rebekah Awood, you have helped guide me on my graduate degree mission since before I was even admitted as a student. I've had countless questions for you over the past four years and in answering them you've always been quick, informative, professional and kind. Thank you for everything you do for students and thank you in particular for all the help you've given me.

Finally, to my colleagues at HARMAN International: thank you all so much for the hard work you put into assisting me with this study and providing the resources necessary to see the work continue. I am proud of what we have accomplished, and I look forward to all that comes next.

Table of Contents

List of Tables

List of Figures

List of Appendices

List of Abbreviations

AC ..... Alternating Current

ANC ..... Active Noise Control

CAD ..... Computer Aided Design

CAE ..... Computer Aided Engineering

CAN ..... Controller Area Network

DAC ..... Digital to Analog Converter

DC ..... Direct Current

DSP ..... Digitial Signal Processing

ECU ..... Electronic Control Unit

EOC ..... Engine Order Cancellation

ESS ..... Exponentially Swept Sine

EV ..... Electrified Vehicle

FIR ..... Finite Impulse Response

FxLMS ..... Filtered-x Least Mean Square

HIL ..... Hardware-in-the-Loop

IR ..... Impulse Response

KPI ..... Key Performance Indicator

LPM ..... Lumped Parameter Model

MCU ..... Microcontroller Unit

NVH ..... Noise Vibration and Harshness

OEM.....Original Equipment Manufacturer

OSB..... Oriented Strand Board

PWM.....Pulse Width Modulation

RNC ..... Road Noise Cancellation

RPM..... Rotations Per Minute

RT60 .....Reverberation Time (60 dB)

SIL..... Software-in-the-Loop

SNR.....Signal to Noise Ratio

SUV.....Sport Utility Vehicle

THD .....Total Harmonic Distortion

TOF ..... Time Of Flight

USB..... Universal Serial Bus

Abstract

This thesis presents the implementation of narrowband (engine order noise target) Active Noise Control (ANC) systems in automotive environments via predictive analysis. This has become necessary to address the rising desires of auto manufacturers to shift further away from development on multiple prototype vehicles and instead towards a completely virtual first phase based on system modeling. This thesis demonstrates that the primary missing element barring a completely virtual ANC system model is the lack of an accurate secondary path estimation (often simply called an impulse response or IR). Included herein is a brief overview of the fundamental technologies and techniques used for much of the ANC industry. A thorough breakdown of the merits of various modeling assumptions with corresponding performance metrics and all coding used to generate the requisite secondary path response relationships. This study concludes that the described methods are fully capable for use with future prototype OEM models to evaluate the integration of narrowband ANC systems. A list of various future research that is made viable through this study is also included.

Chapter 1: Introduction

In recent years, there has been a growing desire among automakers (OEMs) to reduce the number of prototype vehicles created during the earliest stages of the vehicle development lifecycle. The cost of building early prototype vehicles of often very high due to the lack of benefits from the economy of scale (no tooling, hand building components, more manual assembly, etc.). It is also often the case that the value of design iterations and engineering considerations made on vehicles at this stage are limited due to the relative roughness of the overall vehicle condition. Hand made parts or systems generally aren't optimized, making these early prototypes considerably different from their final production intent counterparts when their individual variances are combined into one proof of concept.

This "Design Right First Time" method, however, adds significant challenges for ANC system integrators. It is common practice for ANC suppliers to revisit a vehicle line multiple times during the development lifecycle (often at key milestones) to ensure that the system tuning is well optimized and performing robustly. Robust performance itself is critical since noise content reinforcement can occur if system integration is handled improperly or without an abundance of care. These principles that the OEMs are looking to embrace are without question worthwhile, but it means that the automotive ANC industry must adapt or risk having low system maturity since engineers may only sample from a single pre-production run of vehicles. The author's industry experience in this area gives anecdotal evidence that, for extraneous reasons, when this "one and done" approach has been necessitated in the past that relatively poor outcomes have been noted.

This thesis therefore seeks to prescribe a set of technical methods with which ANC suppliers may appropriately handle this shift. It fully embraces the use of the virtual models which the OEMs are creating or improving. Thereby, these methods enable OEMs and ANC system integrators to proceed with confidence into an era of model-based system testing. Herein shall be presented a recounting of the current industry practices, the ANC system state of the art as well as quantitative comparisons which depict simulation results against real world data. Furthermore, the simulation sensitivity to various modeling elements and decisions are shown coupled with final ANC system noise SPL attenuation values. A brief discussion of future research potential is also presented, all of which is further enabled due to the successful outcomes of this study.

1.1 Current State of ANC Prediction Technology

The overlap between the technical areas of FEA/FEM and ANC predictive technologies are reasonably well studied. Going so far back as the late 1990's and early 2000's, ANC in fully realized 3D environments such as airplane fuselages and heavy equipment operator cabins has been studied through both experimental and finite element methods. It is worthy of note as well that non-FEM numerical methods have been used to analyze ANC going back to the late 1980's. Most notably would likely be the works of Dr.'s Elliott, Bullmore and Nelson [1] [2] [3] who performed some of the earliest modern research into ANC applications and have since furthered their renown in the field.

In their 2003 article, Stanef, Hansen and Morgans [4] provide an in-depth explanation of the technical methods and results that they utilized to optimize the ANC system performance of a mining vehicle cabin. Throughout the literature review conducted to support this study, this article dating back to 2003 remains the closest article of note to the research presented in this thesis.

Stanef *et al.* integrated an ANC system into a modeled cabin and, through the use of FEM, derived secondary path estimates which they then utilized via MATLAB tools to simulate SPL attenuation. The key difference between their work and what is presented here can be clarified as follows: the primary focus of their research was to use the FEA model to support the optimization of ANC being retrofit into an existing cabin. In doing so, they used experimentally derived values and assumptions that would not otherwise be available. The methods presented in this thesis intentionally make no use of such conveniences since, in practice, they would not be available.

Ohadi and Emadi [5] provide explicit techniques of extracting secondary path estimations from FEA models in their 2005 article. Regrettably, this also marks the beginning of a long trend in this field of study where insufficient experimental validation is provided; if any is given at all. While Ohadi *et al.* do provide data describing the SPL reduction of powertrain noise, the powertrain noise is a synthesis of oscillators and the system is never physically realized.

Khatokar *et al.* [6] provide the latest advancements in this field at the time of writing. Their work on using FEA models to simulate secondary path estimations for FxLMS systems utilizes a combined Finite Element Method and Boundary Element Method (FEM-BEM) and a full scale numerical model of the control speakers which enables the evaluation of SPL reduction for control speaker coupling during anti-noise generation. While they did collect experimental data to validate their simulation results, they did not model an actual enclosure and therefore only have experimental data for the speaker responses and no data that depicts a validated vehicle cabin SPL reduction.

Zhang and Wang [7] in their research actually manage to sidestep the need for a secondary path estimation to be calculated and stored entirely. For their novel algorithm which they have dubbed "Deep ANC", they have trained a deep learning model to properly account for the non-linearities

of the electro-acoustic control system instead of relying on measurement data and the FxLMS algorithm. This has presented astounding future potential within the field of ANC research; however, the computational requirements are currently far too high for implementation into most if not all consumer vehicles.

For various reasons, the past decade has had relatively little practical value for FEM enabled ANC system performance prediction. With an abundance of test vehicles and engineering time to commit to solving problems during the development lifecycle of a particular vehicle program, current SIL and HIL technologies that ANC system integrators have access to are used instead to support research or perform system behavior investigations and code validation. Similar to their numerical method counterparts, they have been used as tools to support the study of existing acoustic environments. As such, they also rely on using acoustic measurements as inputs to their models. This fact is what must change to be adequately prepared for the emerging future.

1.2 Matching OEM Needs with Supplier Capabilities

A gap analysis may therefore be applied to the situation at present to determine the core requirements for a set of technical methods to properly address the issues raised here. One may note from the section above that FEA powered models have achieved relatively good SPL reduction predictions, however, they all lack one of two final key elements. They either do not validate with a final system implementation or they include steps which would require access to an already physically realized vehicle cabin which would not exist in the new development lifecycle that OEMs are envisioning. Correction of these two key factors shall therefore be considered critical for a successful outcome.

The process should also include the ability to reproduce all the basic functionality improvements garnered over the past few decades. In short, the following are also considered important outcomes:

- Fully account for the transducers of the ANC system in the model
    - Changes to control speakers and microphones should be easily evaluated to allow suppliers and OEMs to evaluate key component changes
    - Allow for the relocation of control speakers and microphones in the model such that impacts on positioning may be evaluated
- Allow for adjustment of the primary path to simulate the addition or removal of passive NVH enablers
- Allow for the modification of the input signal to accommodate changes in the powertrain design or use of synthesized content
- FxLMS tuning parameters should be easily modifiable to enable the system to be optimized quickly; ideally mimicking the vehicle tuning processes and making them easier and more natural for ANC system engineers to engage with
- Algorithmic behavior should be properly accounted for and modifiable to allow for carryover of this process to future ANC systems (new features, new algorithms, etc)
- and finally, the computational cost to operate should be kept as low as possible while still achieving SPL reduction estimates that are appropriate; thereby allowing for rapid iterating.

The achievement of all these requests is what marks the success of this process and project.

Chapter 2: Technical Background

An overview of the state of the art and other core assumptions is necessary for a complete understanding of the experimental methods to come in the following chapter. Presented here are an overview of the basics of ANC systems, a description of the FxLMS ANC algorithm, the exact definition for the IR input signal (IR chirp), and an overview of the differences between the utilization of the LPM modeling and transfer function convolution methods before ultimately concluding with the post-processing techniques that are being applied to the IRs to prepare them for testing.

2.1 Narrowband ANC Principles

Whereas passive noise control techniques focus on decreasing the energy transmission to a receiver from a noise source by maximizing reflection and absorption in the noise path, active noise control relies on the principle of deconstructive interference. Due to the nature of sound as a mechanical wave, oscillatory energy from multiple sources in space may be summed where their influence overlaps. In the case where a noise and anti-noise source are collocated, so long as the magnitude of the anti-noise is the same and the signal is inverted (180 degrees out of phase), complete global reduction of the noise is achieved (Figure 2-1).

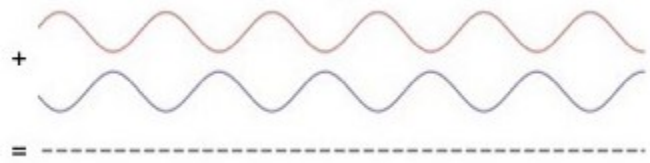

Figure 2-1: Destructive interference of two waves resulting in the complete attenuation of the noise signal [8]

However, in the case of narrowband engine order content, the noise source and anti-noise generating loudspeakers are not collocated. This means that, when control is applied, locations within the environment have the noise content reinforced while some others will be attenuated (Figure 2-2).

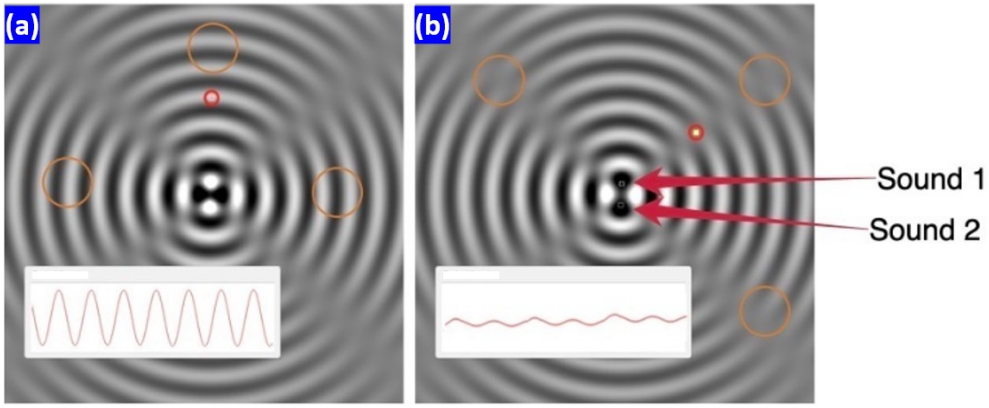

Figure 2-2: A 2D representation of the interference between two noise sources where in (a), the small red circle samples from a region of reinforced noise content and in (b), the red circle samples from a region where noise is attenuated. Orange circles in each show regions where reinforcement or attenuation are similarly occurring [8]

Therefore, it is essential to ensure that the regions where attenuation occurs are located at the occupant's listening locations. In automotive applications, this is approximately the headrests of the seats. Special attention is paid to the driver's seat since it is guaranteed to be occupied during vehicle operation. In order to adjust the location of the attenuation and maximize the level of noise attenuation, the phase of the control speaker signals, their signal magnitudes along and their frequencies must be adjusted to match the harmonic content of the engine. Further adding complication, this varies with engine speed which changes greatly during regular vehicle operation. A control system is therefore used to ensure that the resulting phase and magnitude of the anti-noise is appropriately reducing the target noise for the occupants. Microphones acting as feedback sensors are placed near occupant listening locations (often mounted in the headliner of the vehicle near the occupants' heads) which monitor the treated narrowband noise content in the

frequency range of interest. Since the dominant noise source from the engine of a vehicle is due to the firing of the cylinders, the frequency (in Hz) of the noise source is simply:

$$f = \frac{(Order\ \#)\cdot RPM}{60} \tag{1}$$

The primary firing order (often simply half the number of cylinders of the engine), is the number of combustion events per revolution of the engine and RPM is simply the angular velocity of the engine in rotations per minute. It is often the case that several frequencies of interest will be targeted simultaneously since, in practice, there is also correlated harmonic content associated with this tonal noise. This means that one may define a useful input signal for the control system by monitoring the engine speed and adjusting an oscillator based on the firing order for a particular engine's design. A simplification of a narrowband active noise control system can therefore be constructed from these elements (Figure 2-3).

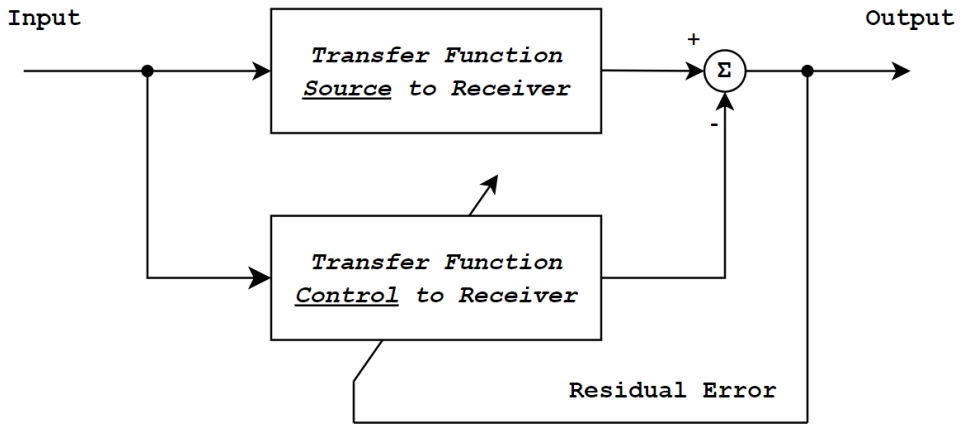

Figure 2-3: A simple block diagram detailing the fundamental organization of the narrowband noise control feedback system

It is obvious then that if the feedback control of the "Control to Receiver" transfer function is well guided, the system will converge such that both transfer functions are identical. This results in complete attenuation of the noise signal. In practice, the "Source to Receiver" is some unknown plant which is characterizable as an acoustic transfer path. Similarly, the "Control to Receiver"

need only be a digital filter of sufficient length whose coefficients are modifiable via the control system. Mathematically, it is possible for an FIR that meets the previously mentioned requirements to have its optimum coefficient vector derived via the solving of a system of linear equations. However, this approach is highly computationally taxing. Instead, an adaptive algorithm approach is used which iteratively improves an approximation until it converges to a near optimum filter.

By creating a cost function based on the size of the residual error from the superposition of engine and anti-noise and seeking to minimize that value, an algorithm may be developed which inherently seeks the optimum filter. However, introducing the electrical domain of the control system does require accounting for. Specifically, this is to account for the electroacoustic transfer function between control speaker signal generation and control microphone sensors and is referred to as the secondary path, impulse response or IR of the system (all synonymous). This is necessary in large part due to the non-linearities at low frequencies of the control system operation. When implemented as described, the error signal therefore becomes:

$$e(n) = d(n) - s(n) * [\omega^T(n)x(n)] \tag{2}$$

Here, $d(n)$ is the engine noise which has already been filtered via the "Source to Receiver" path and is the target for cancellation, $s(n)$ is the impulse response of the "Control to Receiver" path, $\omega^T(n)$ is the transpose of the adaptive filter coefficient vector, $x(n)$ is the input signal vector and n is simply the time step. Further refining the error signal into a usable cost function may be done by calculating the mean square of the error and introducing the steepest decent optimization algorithm which utilizes the negative gradient of the mean square error to provide direction to the updating of the filter coefficient vector (ω^T). This approach leads to the filter update equation:

$$\omega(n+1) \stackrel{\text{def}}{=} \omega(n) - \frac{\mu}{2}\nabla\hat{\xi}(n) \tag{3}$$

$\hat{\xi}(n)$ is the instantaneous approximation of the mean square error ($e^T e$) and μ is an introduced variable often referred to as "step size" which may be modified to increase or decrease the rate of change of the filter coefficient vector. Calculation and expansion of the gradient term using (2) gives:

$$\nabla\hat{\xi}(n) = 2[\nabla \mathrm{e}(\mathrm{n})]e(n) \tag{4}$$

$$\nabla e(n) = -s(n) * x(n) \tag{5}$$

Combining (3), (4) and (5) then gives:

$$\omega(n+1) = \omega(n) + \mu[s(n) * x(n)]e(n) \tag{6}$$

It may be noted then that the filter update equation in (6) is defined wholly by a tunable scalar to adjust adaptation behavior μ, a known system input $x(n)$, the error signal measured by the control microphones $e(n)$ and the unknown impulse response of the secondary path $s(n)$. In cases where the target acoustic environment for ANC treatment physically exists (such as with prototype vehicles), it is a relatively simple task to create an estimation of the secondary path impulse response $\hat{s}(n)$ from a measurement. With this further approximation in place, (6) becomes:

$$\omega(n+1) = \omega(n) + \mu[\hat{s}(n) * x(n)]e(n) \tag{7}$$

This is occasionally further simplified to:

$$\omega(n+1) = \omega(n) + \mu x'(n)e(n) \tag{8}$$

This reflects the fact that $x'(n)$ is simply the input signal $x(n)$ which has been filtered by an approximation of the secondary path's impulse response. This is the foundation of the Filtered-x Least Mean Square (FxLMS) ANC algorithm.

2.2 Basics of FxLMS Systems

The essential knowledge for the implementation of FxLMS for ANC systems may be extracted from Kuo *et al.'s* work presented in 1999 [9]. The elements necessary for anti-noise to be generated are the following (Figure 2-4):

- Primary noise to be canceled (in this case harmonic engine order content); $x(n)$
- An acoustic secondary path; $S(z)$
- An acoustic secondary path estimation (synonymous with IR); $\hat{S}(z)$
- and an acoustic primary path $P(z)$

All other aspects of the system exist and are updated purely within the digital domain; more specifically, they are commonly handled on the DSP chip of the ANC system hardware.

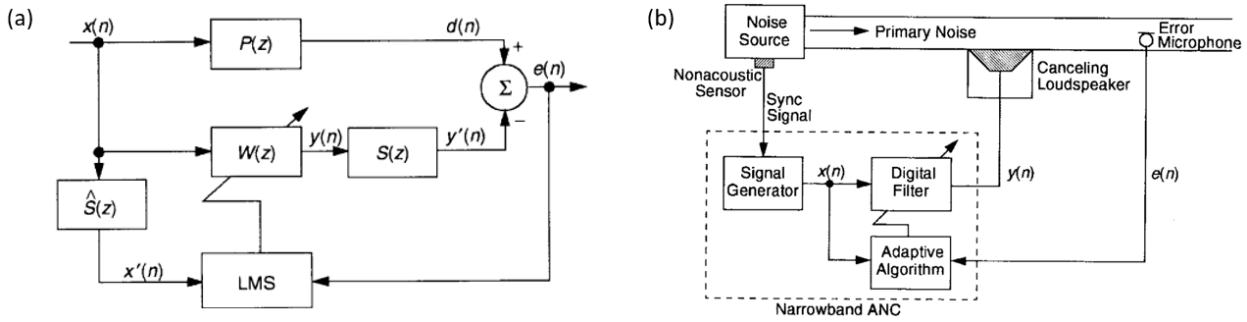

Figure 2-4: (a) Example FxLMS block diagram and (b) a stylized depiction of the FxLMS block diagram which specifically details narrowband cancellation often used for engine order cancellation [9].

One may begin to address each element individually. Primary noise may be generated in several ways. One could, for example capture surrogate noise data from an existing vehicle with similar attributes. For example, a new V8 engine could be approximated by the previously available counterpart. Differences in cylinder displacement are known to affect the amplitude of the signal and therefore appropriate scaling factors could be applied to the signal strength. Alternatively, in narrowband cancellation examples such as we are dealing with here, one could artificially synthesize the primary noise to be cancelled using empirical data and models to estimate signal

strength for the engine order content that is to be attenuated (see Appendix A for a coded example). Finally, if a good quality virtual engine model exists, one could use engine content from that model as a primary noise source. This thesis will explore all but the virtual engine model option.

Describing an appropriate discretized secondary path is, by nature of the problem, a flawed task. One may use an FIR filter that adequately approximates the secondary path for ANC system performance estimation, but this requires assuming that $S(z)$ and $\hat{S}(z)$ are equivalent. If at first that rationale is confusing, it is worthwhile to consider that, if one were to make a more accurate measurement or simulation of the secondary path then the choice to not use it as $\hat{S}(z)$ as well as $S(z)$ is arbitrarily introducing error. The secondary path is a purely physical concept and all improvements to the accuracy of measuring or simulating the secondary path estimation only continue to lower the inherent error between the two. In practice though, this is can largely be ignored. This attitude is taken in part due to necessity, but it also has much to do with the non-linear and time variant nature of the secondary path in all automobiles. Changes in temperature, vehicle loading, varying trim packages and many more variables have been witnessed to have a significant impact on the secondary path. This leads to the conclusion that, for the purposes of this study and in general, it is not improper to simply assume that the two transfer functions are the same so long as the axiom of "garbage in; garbage out" is respected. This thesis will discuss some of these assumptions and their validity later on.

Although the secondary path estimation is normally measured from a prototype vehicle, preparation for the future of "Design Right First" principles require operating under the assumption that prototype vehicles will not be available. Instead, the secondary path estimation may be derived from an FEA model by performing a frequency domain mixed physics simulation. In practice, the OEM creates a CAD model whose material properties and proportions are well defined. Given the

location data of a set of control speaker and microphone locations within the cabin, the acoustic transfer function between each source and receiver may be simulated and has been shown to be dominated heavily by the low frequency acoustic modes [10]. For additional accuracy, one may find it necessary to include the speaker mounting trim and sheet metal stiffness in the model since these structures are mechanically coupled with the control speakers.

The primary path may be estimated in a similar fashion to the secondary path. By including the air space outside of the cabin volume and creating a radiation source in the approximate engine position, one may approximate the acoustic transfer function of the primary path. This may then be convolved with the input signal of the ANC system, thereby providing the "ANC Off" noise levels within the cabin; $d(n)$.

The final user interaction with the simulated system is the tuning of the FxLMS algorithm to achieve maximum system noise SPL attenuation in the frequency range of interest. Specifically, in use for the research presented here is a "leaky" FxLMS system whose filter update equation was derived in the previous section is roughly approximated by the following:

$$\omega(n+1) = \nu\omega(n) + \mu[(s(n) * x(n) \cdot e(n)] \tag{9}$$

ω is a complex filter coefficient vector in the frequency domain. ν is a scalar and represents the leakage term determining how much of the previous filter value is used to define the new value. μ is a scalar referred to as the "step size" which applies a gain to the filter growth term. $s(n)$ is the stored secondary path estimation which is convolved with $x(n)$ (the reference signal vector) which is generated via an oscillator according to the sync signal in the case of narrowband harmonic cancellation. For engine order content cancellation (EOC), this sync reference signal is the RPM signal which is often derived from a pulse signal from the crankshaft encoding wheel which is also known as the "crank signal". Finally, $e(n)$ is the error which is measured via the

control microphones. n is simply a representation of the time index. From this equation, it is clear to see that the only terms which the integration engineer must modify to optimize are the speed and leakage (μ and ν). These therefore are the primary system tuning variables. In practice, other tunable terms are available but vary based on the system design.

2.3 IR Chirp Signal Generation

In [11], Farina details several potential improvements for the measurement of an impulse response via the use of an exponentially swept sine (ESS) wave. His work shows the benefits of this method which are highlighted below:

- Accuracy on par with other common measurement methods
- Provides a quantification of harmonic distortion at various orders
- Ease of use
    - No need for a tight synchronization between the sampling clock and signal generator
    - Pre-recorded excitation signal may be used
- High signal to noise ratio (SNR)
- Functionally immune to time variations of the system under test

For these reasons and the relative ease with which a swept sine input signal may be simulated in the FEA model, the methods prescribed by Farina will be considered for use in this study. The equation used for the creation of the ESS signal is below in (10):

$$x(t) = sin\left[\frac{\omega_1 \cdot T}{ln\left(\frac{\omega_2}{\omega_1}\right)} \cdot \left(e^{\frac{1}{T}\cdot ln\left(\frac{\omega_2}{\omega_1}\right)} - 1\right)\right] \tag{10}$$

ω_1 and ω_2 are the starting and ending frequencies of the chirp and T is the duration of the signal. This chirp is replayed between each control speaker to each control microphone to generate a matrix of secondary path estimates.

2.4 LPM Modeling vs Transfer Function Convolution

This study departs from the methods of other researchers listed in the literature review in a seemingly novel way. The works of the authors described earlier all take measurements of the control speaker's frequency responses and convolve them with the simulated acoustic environment's acoustic secondary path models to achieve a singular measure which contains the near full electro-acoustic transfer function. This method is adequate in that, if nothing else in the electrical domain affects the transfer function, it provides an adequate representation of the secondary path for SPL reduction estimation. Whilst consulting with acoustic modeling industry professionals on this research, it was proposed that a potential benefit might instead be drawn from utilizing FEM in conjunction with a Lumped Parameter Model (LPM acting as a speaker calculator which captures both linear and non-linear speaker behavior [12].

While it is true that use of the LPM method does not allow for the flexibility of individually pairing speaker responses with acoustic transfer functions, the benefits gained more than offset this detriment. In service to one of this study's primary objectives, the LPM method makes it very easy to simulate speaker characteristics for a module that does not yet physically exist. Because the LPM method utilizes electromechanical parameters of the speaker as inputs. One may either input the parameters for a speaker which has been specified for use or alternatively use the design intent parameters for speakers not yet produced. This further allows analysis of the impact on changing various speaker parameters directly on the ANC system functionality. Other fringe benefits include

the simple fact that an LPM/THD speaker calculator is already integrated into COMSOL Multiphysics and that COMSOL is an industry standard modeling software used by audio system suppliers (automotive ANC system suppliers being predominately audio system suppliers first and foremost). This enables system suppliers to simply further their use of COMSOL, a modeling software package with which they are already likely highly familiar. In fact, if an audio/ANC system provider is already providing their OEM customers with high quality audio system auralizations then they are functionally reproducing the secondary path with reasonable accuracy.

2.5 IR Post-Processing

In a follow-up article written in 2007, Farina [13] provides additional refinements to his original paper on the subject of the ESS IR measurement method. Many of the updated recommendations that Farina prescribe are irrelevant when considering a virtual frequency domain model such as mismatching of playback and recording clocks, pulsive noise during system response recordings and transducer electromechanical considerations. However, Farina does recommend a frequency response envelope to be applied to address pre-ringing concerns in physical measurements. Because of the nature of this study's comparison of the experimentally derived IR using Farina's method and the simulated IR, the same frequency enveloping will be applied to the simulated results.

Furthermore, it is notable that COMSOL does not estimate Time of Flight (TOF) in providing the simulated IR data. Therefore, the time domain results of the simulation are upsampled to a much higher sampling rate and leading zeros are added to the data to simulate the proper TOF before being downsampled again. An example MATLAB script that performs all of these post-processing tasks is provided in Appendix B.

Chapter 3: Experimental Methods

Featured in this chapter is a comprehensive overview of the specific research design details of this study. Presented chronologically with accompanying rationale are the design of a test cabin and all included features, the selection of a control loudspeaker, an overview of the modeling along with validation steps, the collection of surrogate primary noise and final integration of all components.

3.1 Testing Enclosure Design

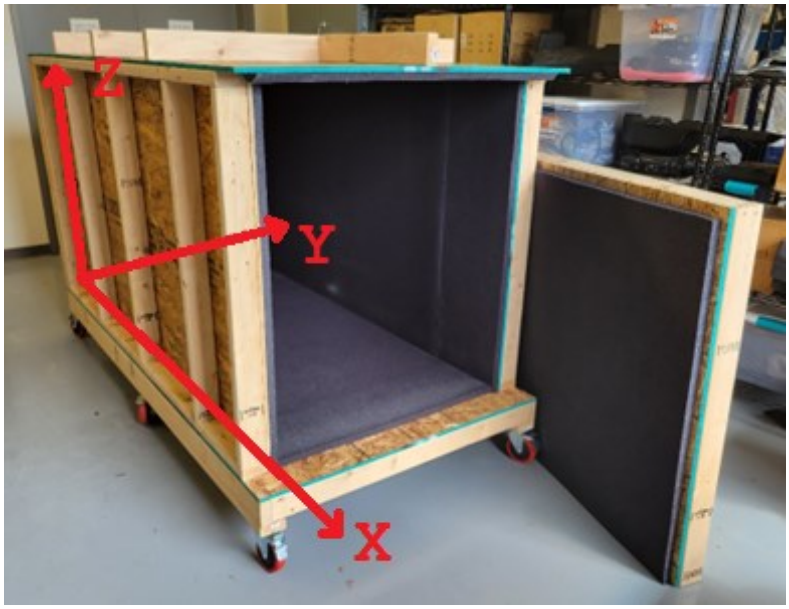

Figure 3-1: Physically realized enclosure design to be modeled for use in FEM analysis. The origin of all referenced coordinate systems in this thesis is the intersection of all the axis shown above in red.

Pictured above (Figure 3-1) is the test enclosure that was prepared for the experimental validation of this study. The enclosure is framed using pine studs with ½ inch OSB and lined with one-inch-thick acoustic foam on all interior faces. This section will discuss the design considerations for the

enclosure itself along with the testing done to ensure that it has acoustic properties of roughly the same order as an automobile cabin. Furthermore, special care is given to how the exterior environment of the test site is prepared along with providing electrical power.

This thesis will also refer to the dimensional axes X, Y and Z. This is made consistent throughout all tables and figures and the origin of this coordinate system is the corner of the enclosure furthest from the door on the bottom left (from the perspective of looking in from the doorway).

3.1.1 Dimensional Considerations

For the benefit of the reader, it may be useful to refer to Appendix E which provides detailed illustrations of the enclosure including its dimensions and construction which will otherwise only be discussed in this section.

The primary considerations for the enclosure design were quite simple. Ease of creation and modeling was primary. By using a basic “two foot on center” framing method along with pine 2x4 studs and ½ inch OSB sheeting, each panel (base, two long walls, one short wall, a ribbed roof, and a simple door) could be fabricated quickly outside of the lab environment and then screwed together in location to keep dust at a minimum. The secondary goal was to give the enclosure dimensions which are roughly appropriate for an automotive environment.

This approach to ordering design priorities leads to the obvious concern that there does not exist a consumer automobile with no interior features, these somewhat odd dimensions and with parallel faces. However, approaching the goals of the study wholistically, one may note that adding more features to the enclosure does not make the results more rigorous and only acts to increase labor on construction and modeling. Of primary concern here is the difference between a measured and

simulated secondary path estimation being low. The secondary path approaching that of an actual vehicle is therefore secondary because it is not novel. It should also be noted that the locations of transducers and speaker orientation contribute far more to the features of the secondary path estimations.

3.1.2 Control Loudspeaker Selection

The ideal for the selected control loudspeaker would be a subwoofer that has low THD in the frequency range of interest for cancellation (from about 35 to 250 Hz). It is often the case that premium ANC applications will use the subwoofer from the vehicle's audio system to drive much of this low frequency energy. Keeping automotive grade components and practices a priority wherever appropriate therefore pointed towards selecting a well-studied vehicle speaker that managed low frequency performance well. After some review of potential options, a 10-inch diameter round rear deck subwoofer was selected (Figure 3-2). The fundamental SPL and THD measurements of this speaker are also noted here and are considered sufficient based on the identified metrics above for this study (Figure 3-3).

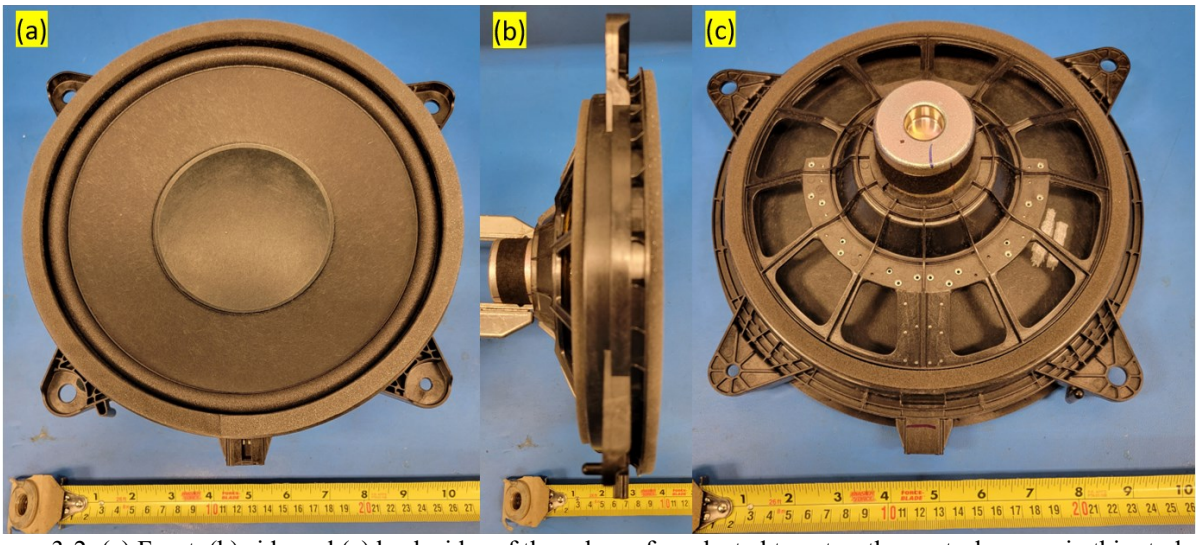

Figure 3-2: (a) Front, (b) side and (c) back sides of the subwoofer selected to act as the control source in this study.

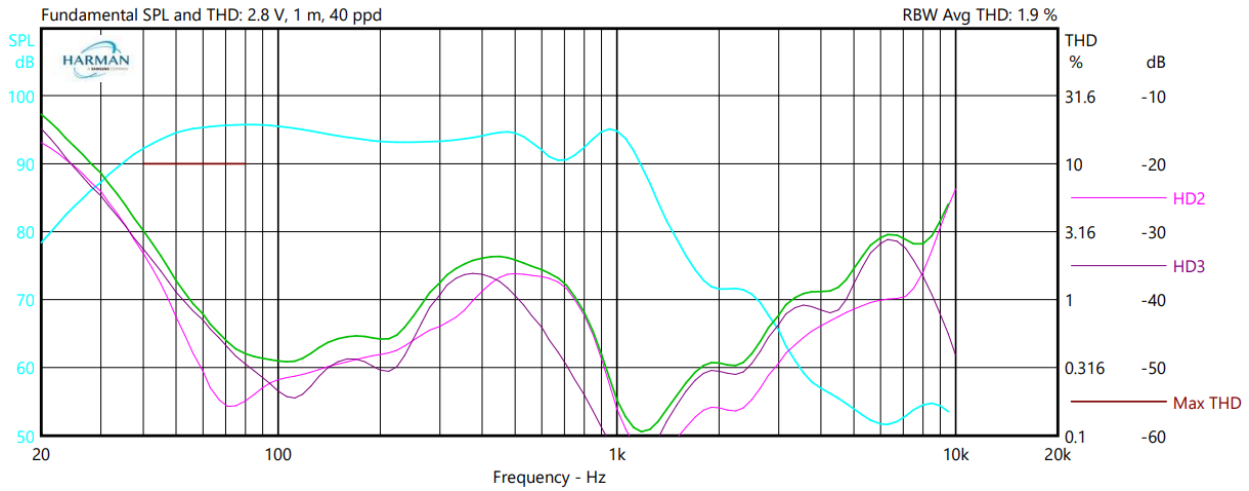

Figure 3-3: Fundamental SPL and THD for the selected control loudspeaker as a function of frequency. This data shows less than approximately 5% THD in the frequency range of interest across all measurements which is considered sufficient quality to proceed [14].

3.1.3 Transducer Placement

For packaging and ANC system performance reasons, a common compromise for placing control microphones in the cabin of an automobile is to embed them in the headliner. More precisely, it is noted that using microphone locations closer to the corners of the cabin volume is preferable for ANC performance [2]. There is a trade-off in practice of placing microphones in the furthest extents of the enclosure, however. It has been shown that in instances where the control and primary sources are not collocated, such as it is the case here, there is an effective spherical zone of cancellation around each control microphone. The radius of this quiet zone is approximately one tenth of the wavelength of the noise to be attenuated [15]. Therefore, there exists a optimal location between the occupant's listening position and the corners of the enclosure where potential for SPL reduction is a maximum. For this study, the control microphone locations in the front (furthest in the X-axis) of the enclosure were selected somewhat arbitrarily while still following these guidelines. Considering the author's past experience with negotiating control microphone

locations with OEMs, the locations chosen are appropriate and reflect where the automakers would likely permit them to be placed.

The control microphones closer to the midpoint of the enclosure (approximating a rear seating location in a vehicle with rear storage space) differ from the prior guidelines somewhat. Because the supposed occupant seating location is much farther from the front or rear of the acoustic environment, it is instead worthwhile to rely on a different principle. The control microphone locations are instead pulled closer towards one another. This means that the effective quiet zones begin to overlap. Due to the tendency of FxLMS systems to weight performance at all microphone locations equally, one may effectively increase control effort towards the overlapping region of influence. Often, this is accomplished without any degradation of system performance in the front listening locations.

The relatively large size of the quiet zones at low frequencies permits one to expect to see similar levels of SPL reduction in large areas inversely proportional to the frequency of interest. Therefore, only a few microphone locations need to be instrumented for the recording of ANC on and off states. In total, seven random incidence microphones are placed in the enclosure, four of which are collocated with the control microphones which are relatively cheap analog microphones designed for use specifically for use in automotive ANC applications (Figure 3-4).

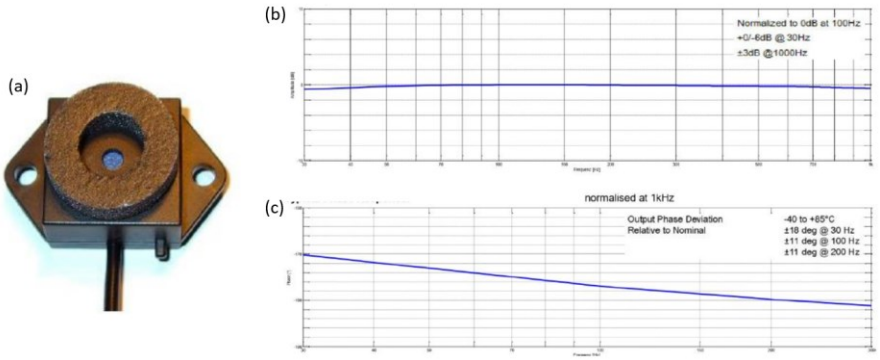

Figure 3-4: (a) Control microphone, (b) magnitude response and (c) phase response corresponding to said control microphone.

For the benefit of the reader, the system coordinates of all control and measurement microphone locations are detailed (Figure 3-5) here along with an explanation of all sensors located at each label (Table 3-1).

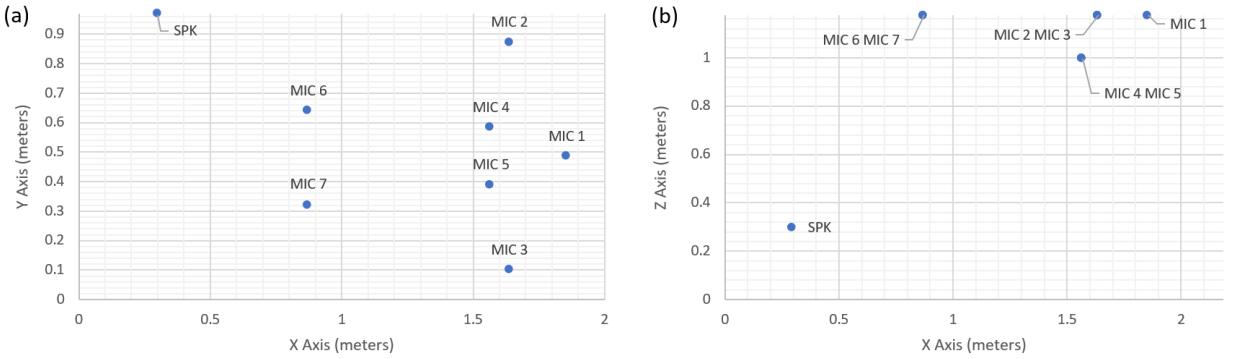

Figure 3-5: (a) Projection of all transducer locations onto the X-Y plane (top view equivalent) and (b) a projection of all transducer locations onto the X-Z plane (side view equivalent).

Table 3-1: Dimensions and coordinates of free acoustic space of enclosure and all transducers respectively (includes detailing of which sensors are collocated)

Axis	Acoustic Volume Dimensions (m)
X	2.184
Y	0.965
Z	1.175

Label	X Coor. (meters)	Y Coor. (meters)	Z Coor. (meters)	Measurement Microphone #	Control Microphone #
MIC 1	1.8564	0.4825	1.175	1	None
MIC 2	1.638	0.8685	1.175	2	1
MIC 3	1.638	0.0965	1.175	3	2
MIC 4	1.568	0.579	0.9972	4	None
MIC 5	1.568	0.386	0.9972	5	None
MIC 6	0.8736	0.6369	1.175	6	3
MIC 7	0.8736	0.31845	1.175	7	4
SPK	0.7736	0.4825	0.9972	N/A	N/A

3.1.4 Rigidity and Stiffening Members

An original assumption of the study was that it would be reasonable to approximate the enclosure as infinitely rigid for the purposes of simplifying the modeling process. This removed the need to take the coupling of the wall and the control speaker into account. Additionally, the adding of stiffening members greatly increases the robustness of the full assembly which aids in making the environment safe to enter while placing control sensors and preventing damage while moving into

and out of the test environment. A collection of illustrations detailing the dimensions and materials is available in Appendix E.

After the first round of results analysis was conducted, it was ultimately determined that the assumption of an infinitely rigid enclosure was inappropriate. The lower stiffness of the wooden construction along with the relatively high energy recording of surrogate noise led to significant interactions between the enclosure wall and the control loudspeaker. A more complete analysis of this interaction is presented in Section 4.1.1.

3.1.5 Acoustic Treatment

As mentioned in prior sections, all surfaces in the enclosure are treated with a covering of one-inch-thick acoustic foam. While not strictly necessary, the inclusion of this feature into the design aids in a few key ways. First and foremost is the impact on secondary path measurement accuracy. As Farina details in his 2007 article [13], negative impacts on impulse response accuracy are noted when reverberation time is sufficiently long to exceed the recording length employed by the module. The acoustic energy should ideally fade out entirely and end in a zero crossing to ensure that there is not a "clip" which would introduce broadband noise in the measurement. The untreated enclosure would have very low absorption and dampening of the acoustic energy which could lead to reverberant tails of the IR chirp signal cutting off early.

While keeping the parallel goals to acoustically treat the surfaces and keep modeling simple in mind, it was decided that all surfaces should uniformly be coated in acoustic foam to approach an RT60 value which was below the one second impulse response recording length and which approached that of a typical vehicle environment. Hence, large sheets of acoustic foam were cut down to size to fit all the internal surfaces and adhered with foam safe spray adhesive (3M

Super77). See Appendix F for details on the mechanical and acoustic properties of the selected foam.

3.1.5.1 Reverberation Time Matching

With a random incidence microphone instrumented centrally in each environment, a balloon pop recording was made in both the test enclosure with one inch of acoustic foam treatment and the interior of a mid-size SUV using a HEAD Acoustics frontend. Both datasets where then imported into Artemis Suite (post-processing software from HEAD Acoustics) and the "Reverberation Time vs Band" analysis was utilized with a 5dB decay measurement start threshold and a 40dB decay range over the measurement. The analyses were then overlayed with each other and are presented here (Figure 3-6).

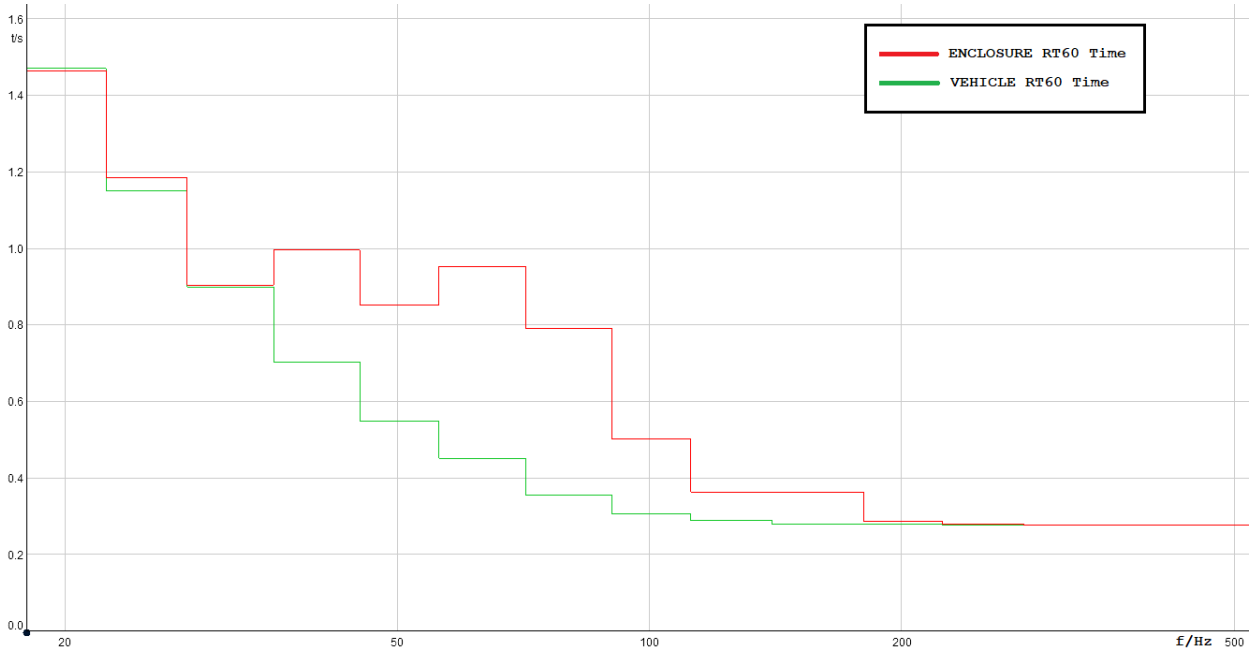

Figure 3-6: Reverberation time (RT60) measured in the test enclosure with one inch of acoustic foam treating all surfaces (red) and in a mid-size SUV (green). Output from Artemis Suite "Reverberation Time vs Band" analysis. Depicts results in 1/3 octave scale.

As one may see from the data, the enclosure with one inch of acoustic foam treatment remains more reverberant than the test vehicle. That being said, the analysis concludes that the impulse response measurement should suffer little to no impact due to all RT60 times being at one second or below. One may also intuit that additional treatment would likely not significantly improve the matching between the two environments. The increase in reverberation time is predominately due to the presence of strong structural and acoustic resonances in the enclosure which would require significant amounts of treatment material. This would cause other more important acoustic properties to vary further away from resembling a vehicle and therefore the amount of treatment was kept at one inch thick.

3.1.6 Test Environment

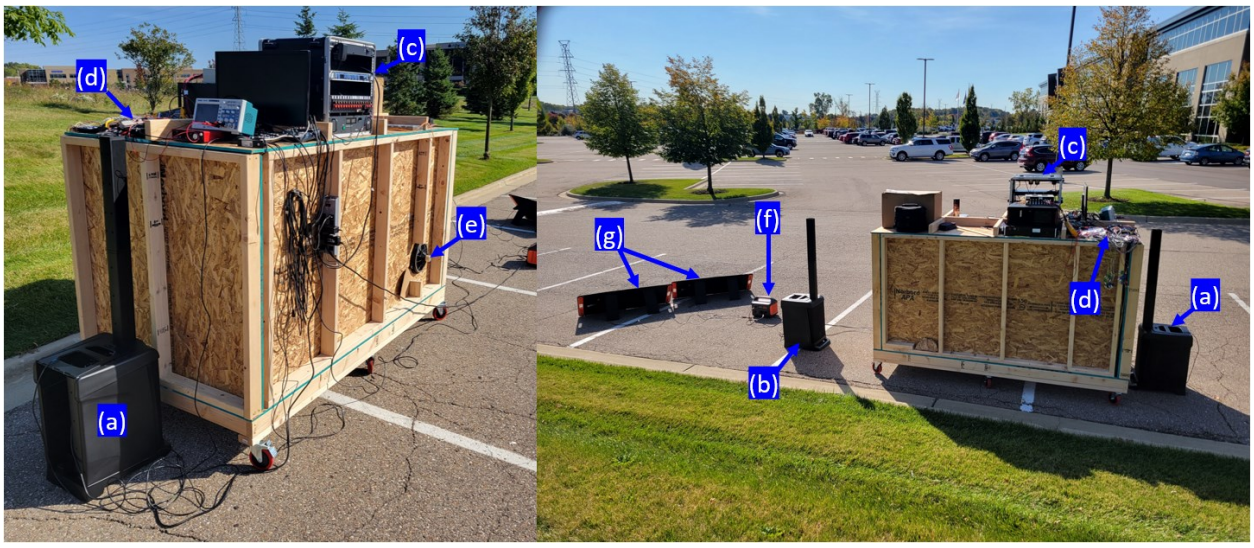

Figure 3-7: Depiction of the free-far field test environment complete with (a) the JBL EON ONE responsible for engine primary noise playback, (b) a second JBL EON ONE loudspeaker for exhaust primary noise playback, (c) the audio rack containing playback equipment and a 13.7V power supply, (d) the ANC demonstration hardware, (e) the placement of the control loudspeaker, (f) the Jackery Explorer 1000 solar generator and battery bank and (g) the accompanying solar panels used to maintain the charge on the Jackery Explorer 1000 while not testing.

As shown (Figure 3-7), all testing was conducted outdoors to approximate a free-far field environment. On a day with acceptable weather conditions, the enclosure loaded with all necessary

equipment may be pushed into a satisfactory location and deployed as seen. Remote power is supplied via a battery bank to all electrical components and all necessary signal routing connections are made. Once setup is complete, a Squadriga II (not pictured) is connected to all measurement microphone locations in the enclosure. All data connections necessary for the ANC demonstration hardware, Squadriga II, playback system and CAN module are then connected via a USB hub and a long USB extension cable to the controlling laptop running all software and analysis.

Outdoor noise pollution was considered as a factor to measure during this study, however, it was ultimately decided that it would be unnecessary. This research was primarily conducted during the large societal shift towards working from home and therefore very little ambient noise was noted. Start of recording was triggered by microphone pressure level thresholds and all runs where errant noise was detected by the test operator were restarted. Between the relatively quiet test environment and good isolation provided by the test enclosure itself, the interior of the enclosure had a considerably low noise floor. Furthermore, due to the bandpass filtering done on the microphone lines on narrowband cancellation ANC systems, only noise at the same frequency that the system was attempting to cancel would be of a concern. Extra precaution to ensure a quiet environment was taken during all impulse response measuring steps.

3.1.7 Power Supply Considerations

Supplying the electrical systems of the test setup required special consideration. Due to testing in the outdoors, access to electrical power was not readily available. Running the necessary length of extension chord to the test site would be impractical and potentially dangerous once higher energy demands would be necessary. Conventional gas or diesel generators are also not appropriate for

the application due to the high level of noise they produce while operating. A battery power solution therefore had to be devised which could support the test site. Adding further complication is the need for multiple voltages simultaneously to run the various equipment. Luckily, new "off-the-shelf" solutions have become commonplace that can satisfy these needs.

All electrical power for testing was provided via a "Jackery Explorer 1000 Solar Generator". The device comes equipped with a 1000Wh battery capacity and enough discharge rate overhead to properly supply all systems. Important as well is the fact that this model comes equipped with a "Pure Sine Inverter", meaning that the 110V AC power does not carry a lot of electrical noise that cheaper inverters supply. The high capacity and ability to attach up to 200W of solar panel charging meant that even over the course of a twelve hour test day the battery capacity would only diminish by about ten to twelve percent. This AC source also provided power for a 13.7V DC power supply which then supplied all components made to run off of a vehicle battery or alternator. The final consideration was to make sure that all test hardware, including the test operator's laptop, were powered from this battery bank to avoid multiple ground states which can cause noise in audio systems.

3.2 FEA Model Creation

The air volume within the enclosure was modeled via a simple rectangular prism in CATIA V6. This model was then exported to COMSOL Mutliphysics where the beams, meshing, LPM speaker parameters and materials properties were defined (Figure 3-8). Using a 0-300Hz frequency range with a 2Hz frequency step, the secondary path estimations between the control loudspeaker position and control microphone positions were calculated.

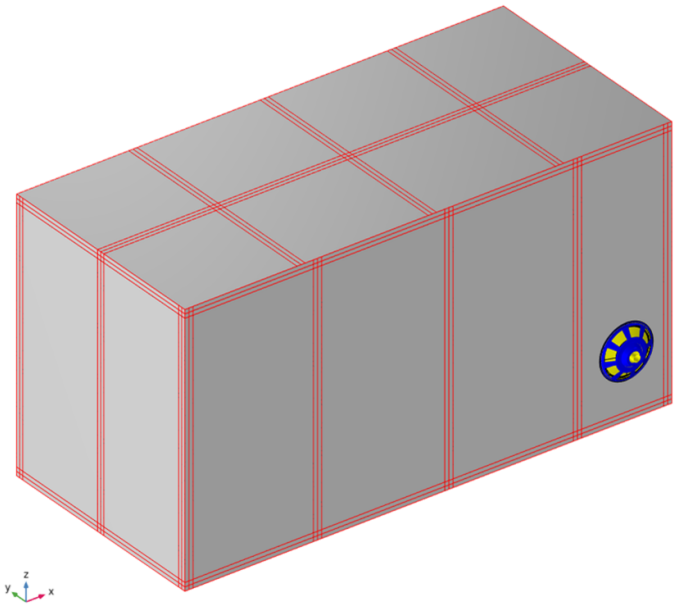

Figure 3-8: FEM Beam Model of the enclosure used for calculation of the acoustic secondary path estimations

The OSB sheeting was modelled as a shell component. Since material properties databases have limited usefulness in applications involving wood, approximate measurements were needed for critical values. The density of the OSB was measured to be approximately 690 Kg per cubic meter. The Young's modulus was set to a common value of 900 MPa. Poisson's ratio was approximated to 0.25. The pine 2x4 studs, being far more rigid than the OSB sheeting, simply had their stiffnesses set to very high values.

With the model prepared, a modal analysis of the acoustic cavity was conducted to ensure that the low frequency resonances and their appropriate resonant frequencies were detected. This is presented in the next section.

3.3 Preliminary Model Validation

One of the largest benefits of choosing a rectangular enclosure is that many analytical models developed for use in rooms are applicable here as well. To validate the preliminary modal analysis

study conducted in the previous section, one may compare the eigenfrequencies and their corresponding mode shapes with those from the equation for the eigenfrequencies of a rectangular room f_λ, shown below:

$$f_\lambda = \frac{c}{2}\sqrt{\left(\frac{M}{l}\right)^2 + \left(\frac{N}{w}\right)^2 + \left(\frac{P}{h}\right)^2} \tag{11}$$

Here, c is the speed of sound in air, $M,\ N,\ P$ are the X, Y and Z axis mode numbers respectively and l, w, h are the enclosure free air space length width and height (corresponding to the X, Y and Z axis) respectively. Therefore, through creating a calculator for eigenfrequencies as a function of mode numbers and sorting the results one may determine the mode shapes of the cabin as a function of eigenfrequencies. The code used to conduct this search is provided in Appendix D. The first ten results from the sorted search (up to 237Hz) is presented below (Table 3-2):

Table 3-2: Comparison of FEA Output with Analytical Model

Analytical Sorted Eigenfrequency (Hz)	Analytical X-Axis Mode #	Analytical Y-Axis Mode #	Analytical Z-Axis Mode #	Simulated Eigenfrequency (Hz)	Simulated X-Axis Mode	Simulated Y-Axis Mode	Simulated Z-Axis Mode
78	1	0	0	79 (+1.3%)	1 (MATCH)	0 (MATCH)	0 (MATCH)
145	0	0	1	147 (+1.4%)	0 (MATCH)	0 (MATCH)	1 (MATCH)
157	2	0	0	158 (+0.6%)	2 (MATCH)	0 (MATCH)	0 (MATCH)
165	1	0	1	167 (+1.2%)	1 (MATCH)	0 (MATCH)	1 (MATCH)
177	0	1	0	179 (+1.1%)	0 (MATCH)	1 (MATCH)	0 (MATCH)
194	1	1	0	196 (+1%)	1 (MATCH)	1 (MATCH)	0 (MATCH)
214	2	0	1	216 (+0.9%)	2 (MATCH)	0 (MATCH)	1 (MATCH)
229	0	1	1	232 (+1.3%)	0 (MATCH)	1 (MATCH)	1 (MATCH)
235	3	0	0	237 (+0.8%)	3 (MATCH)	0 (MATCH)	0 (MATCH)
237	2	1	0	239 (+0.8%)	2 (MATCH)	1 (MATCH)	0 (MATCH)

Two important facts may be noted from this data. First is that the error of the simulated eigenfrequency does bias high but is consistently 1.3% different or lower in the range analyzed. Second, is that all acoustic modes are properly detected and appear in the correct order. Since these modes greatly impact the secondary path of the system, the tight matching of the analytical model is an indication that the simulation model is sufficiently refined to continue with further analysis.

3.4 Surrogate Primary Noise Measurement

In the instances where the use of surrogate primary noise from an existing vehicle is desired, it is recommended to capture both engine and exhaust tones at the source such that the recordings contain as little influence from the primary path as possible. Illustrated here is an example setup that corresponds to the surrogate primary data collected for this study (Figure 3-9).

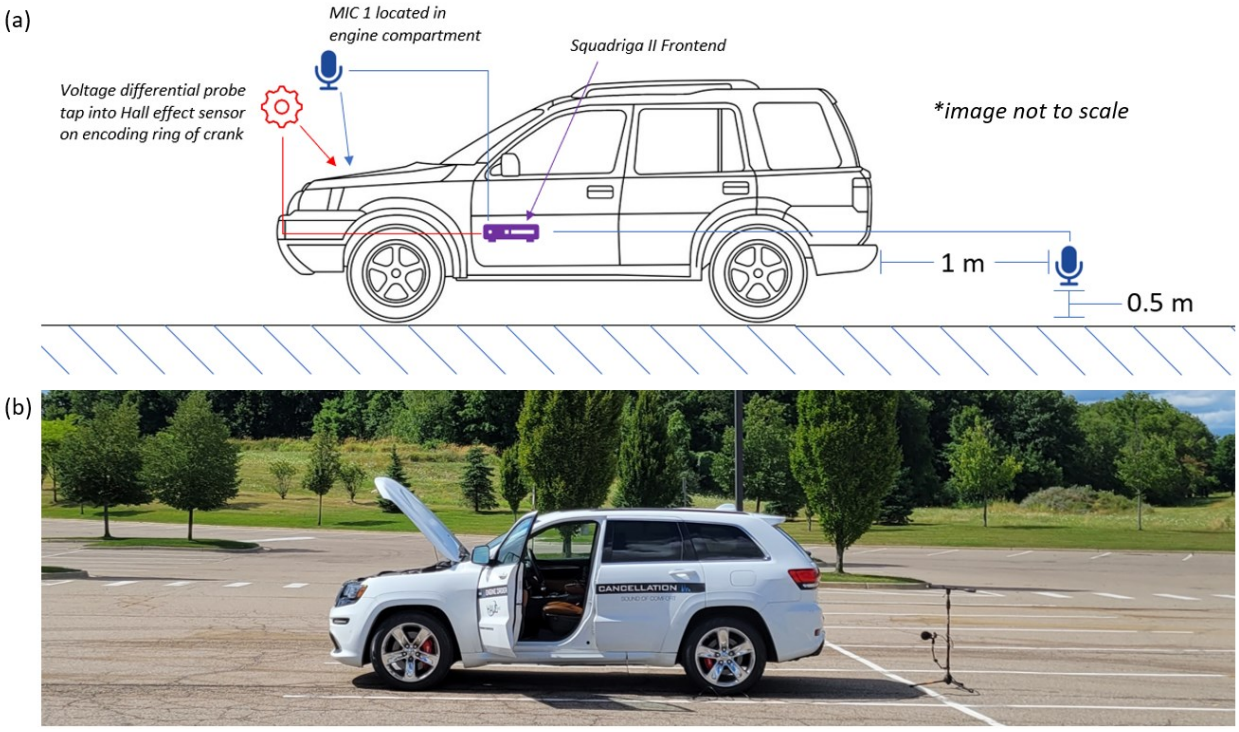

Figure 3-9: (a) Illustration of hardware installation for surrogate noise data collection and (b) photo from surrogate primary noise data collection (hood and door closed during all measurements)

As one may note from the illustration, the recording of the primary noise is simple. The engine compartment microphone is placed in an empty cavity just next to the cylinder head while the exhaust microphone is simply directed straight at the exhaust outlet. Both microphones have attached windscreens to protect from buffeting due to wind or the radiator fan. The output leads from the Hall effect sensor on the engine's encoding wheel are then tapped into and connected to a KEYSIGHT N2791A 25MHz High Voltage Differential Probe. Power for the voltage probe is provided via USB from the media console and the probe output is connected to the Squadriga II

so that both microphone channels and the crank signal are collected simultaneously. On this particular model of voltage probe, the lowest signal attenuation possible is 10:1 and therefore a simple correction is made in the channel list to appropriately gain the recorded file back to 1V/V.

While this method for collecting primary noise data does not require a test track due to being entirely stationary, it does mean that the noise recorded will not exhibit the same sound qualities of an engine under load. Regardless, with the recording armed, one may then manually manipulate the RPM of the vehicle using the gas pedal and a careful operation. The RPM ramp up profile used for the tuning and final system performance measurements of this study is presented here (Figure 3-10).

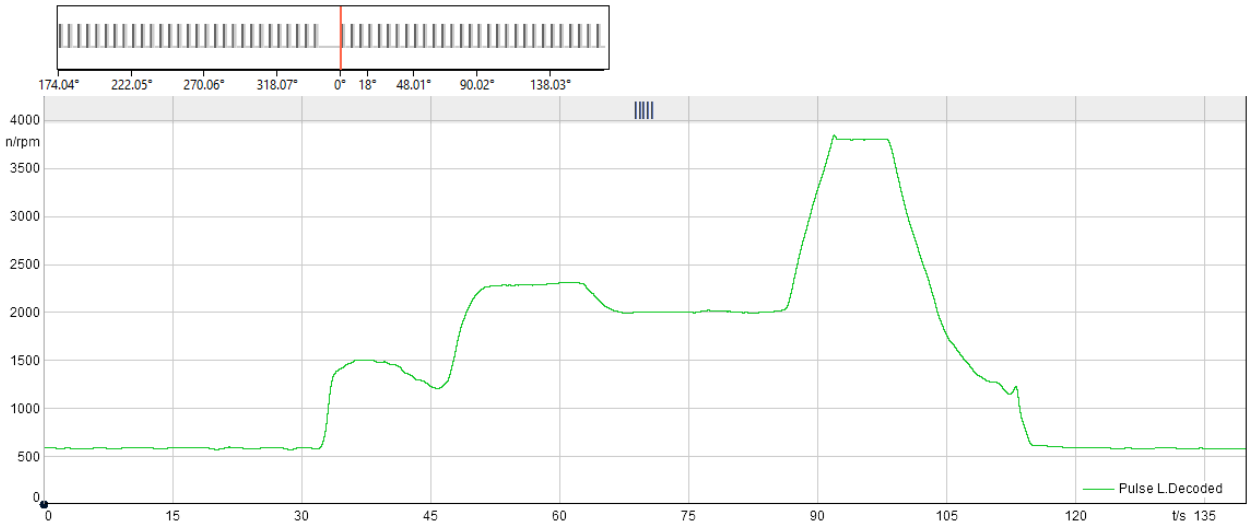

Figure 3-10: Surrogate primary noise RPM profile. Reconstructed from pulse data using a 60-2 zebratape configuration in Artemis Suite.

The recording starts and ends with the vehicle at idle, increases to approximately 1500, 2250, 2000 and finally 3800 before ramping back down slowly to idle. This is done to capture the dynamic behavior of the ANC system during testing and ensure that the entire operating range for ANC is being evaluated. This SUV is equipped with a V8 engine and therefore primary firing order is 4th engine order. Once all data collection is completed, the recording is then exported from Artemis Suite and into separate 48KHz .wav files to later be used by the playback system.

3.5 Synthesis of Virtual Engine Order Content

If access to an appropriately similar donor vehicle is not possible or undesirable for some other reason, the synthesis of virtual engine order content is an option. The only true requirement is that the noise be generated with a correlated sync signal when using the narrowband FxLMS system. In practice, the equation to calculate a single oscillator as a function of time and engine RPM is merely a modification of the equation for a sinusoidal signal, see below:

$$x(A, n, RPM, t) = A \sin\left[2\pi n \left(\frac{\text{RPM}}{60}\right) t\right] \tag{12}$$

A is the desired signal amplitude (recommended to be no greater than one), n is the firing order of the oscillator desired, RPM is the engine rotation speed (in revolutions per minute) and t is time in seconds. When discretized (see Appendix A for an example), the RPM of the equation may instead be a vector. Vectorizing RPM allows for the RPM to vary over the synthesized recording which allows the user to define sweeps. Static RPM will be used in all instances of synthesized engine order content in this thesis due to the availability of the surrogate noise data collected.

Via the principle of superposition, multiple of these sinusoidal oscillators may be summed together to produce additional harmonic content. In practice, if one chooses this approach, some further realism may be added by varying the sinusoid amplitudes in order to reflect engine noise profile characteristics. Additionally, summing of some amount of pink or brown noise into the final signal gives a noise floor for the ANC system to contend with which is far more realistic than pure tones.

Ultimately, this method of primary noise synthesis should be considered a last resort or used when the system operator or engineer is aware of a specific reason why it should be used instead. Surrogate engine order content is relatively simple to record and the output from a virtual engine can provide a much more realistic result.

3.5.1 Sync Pulse Creation

To aid the understanding of this section, the reader may find it valuable to periodically refer the code example provided in Appendix A. The logic used to construct the synthesized crank pulse which correlates with the synthesized primary noise relies heavily on logic statements and is based on the angular frequency of the imagined engine. When assuming the most difficult case in which a dynamic RPM is desired, one must first create that RPM profile. This may be done trivially in a variety of different ways and therefore is not covered here but special care should be taken to ensure that the RPM profile is a timeseries with a common sampling rate to that which is used by the data preparation and writing script (16384 samples per second in this case; capable of handling up to approximately 8000 RPM without significant error). Once a suitable RPM profile is available the unwrapped phase of the crank profile may be calculated via discrete integration.

$$\phi(t) = \frac{1}{f_s}\sum_{i=1}^{t}\left(\frac{360 \cdot RPM(i)}{60}\right) \quad \text{or,} \quad \phi(t) = \frac{6}{f_s}\sum_{i=1}^{t}(RPM(i)) \tag{13}$$

Evaluated at all time steps t, ϕ becomes a timeseries of the phase angle of the engine in degrees. It is understood that the encoding wheel attached to the crankshaft of engines often follow the 60-2 standard and therefore a series of modulo operators and logic statements may be used to turn ϕ into a time series of pulses which replicates the Hall effect sensor output which the ANC module is expecting. First, ϕ is converted into its wrapped form via the modulo operator:

$$\phi_{wrap}(t) = \phi(t)\ mod\ 360 \tag{14}$$

To simulate the missing two teeth of the encoding wheel profile, all values of wrapped phase that are greater than 345 degrees are set to an arbitrary value close but not equal to 360 degrees (359 in the example). This ensures that no logic high will be set in this phase range during future

operations since the encoding wheel is assumed to be at the leading edge of the first tooth after the gap at $t(0)$.

$$\phi_{wrap}(t) > 345 \stackrel{\text{def}}{=} 359 \tag{15}$$

Now, individual tooth and gap pairings may be obtained by performing another modulation operation every six degrees.

$$\phi_{tooth}(t) = \phi_{wrap}(t) \; mod \; 6 \tag{16}$$

At this point, $\phi_{tooth}(t)$ is a timeseries of values ranging from zero to six where the first three degrees reflect a missing tooth and the later three degrees are where a tooth is present. For convenience, subtracting all elements of $\phi_{tooth}(t)$ by three makes this shift in behavior a difference between positive and negative values (now ranging between negative three and three). Furthermore, due to the assumptions used to establish the missing tooth pairing and encoding wheel position at time $t(0)$ it is beneficial to invert the signal as well by multiplying by a negative one which is enabled by removing the signal average.

$$\phi_{tooth}^{-1}(t) \stackrel{\text{def}}{=} -1 \, [\phi_{tooth}(t) - 3] \tag{17}$$

Once in this form, the Hall effect mimicking pulse train $x(t)$ may be created by assigning all values in the $\phi_{tooth}^{-1}(t)$ timeseries to a logic high or low depending on whether the value is greater than zero or less than or equal to zero respectively.

$$x(t) = 0 \quad \text{at all values } t \text{ where,} \quad \phi_{tooth}^{-1}(t) \leq 0 \tag{18}$$

$$\text{and,} \quad x(t) = 1 \quad \text{at all values } t \text{ where,} \quad \phi_{tooth}^{-1}(t) > 0 \tag{19}$$

When writing $x(t)$ to a .wav file, it is beneficial to decrease the signal amplitude by performing an element wise scalar multiplication of 0.9 or some other value slightly lower than one. This is to

prevent errors due to the signal clipping. Ultimately, the signal amplitude will be boosted via the playback system to the nominal crank signal values ranging from logic low at 0V and logic high at 5V that the ANC system expects.

3.6 Playback System Integration

While time synchronous playback of multiple .wav file may easily be achieved via modular audio software application such as AudioMulch, the crank signal represents a unique challenge in that it's voltage range of zero to five volts means that soundcards won't be able to reproduce the signal with the proper amplitude necessary for pulse logic detection. One may consider solving this challenge by employing amplification circuitry, however, this present another challenge in that the development of a low noise amplification circuit with a very consistent delay is required which must then be calibrated. Instead of that option, the work of primary noise and crank signal playback is controlled in this research via National Instrument's LabView software and an accompanying CompactDAQ equipped with an NI-9269 four channel analog voltage output module. The compactDAQ and module are installed into the audio rack on top of the enclosure with the first three channels wired to the engine speaker, exhaust speaker and crank signal wire of the ANC demo hardware respectively. A simple LabView project is then created to support the .wav file playback through the voltage output module (Figure 3-11).

From the LabView signal flow, one may provide all the necessary signal file paths and then adjust the signal gain and delay using the control signal scaling and delay blocks. While monitoring the level inside the enclosure, the gain levels were adjusted such that the energy reasonably matched what was present inside the vehicle cabin during primary noise data collection. The crank signal

strength was adjusted until the output was clearly the intended zero to five volts as measured via an oscilloscope.

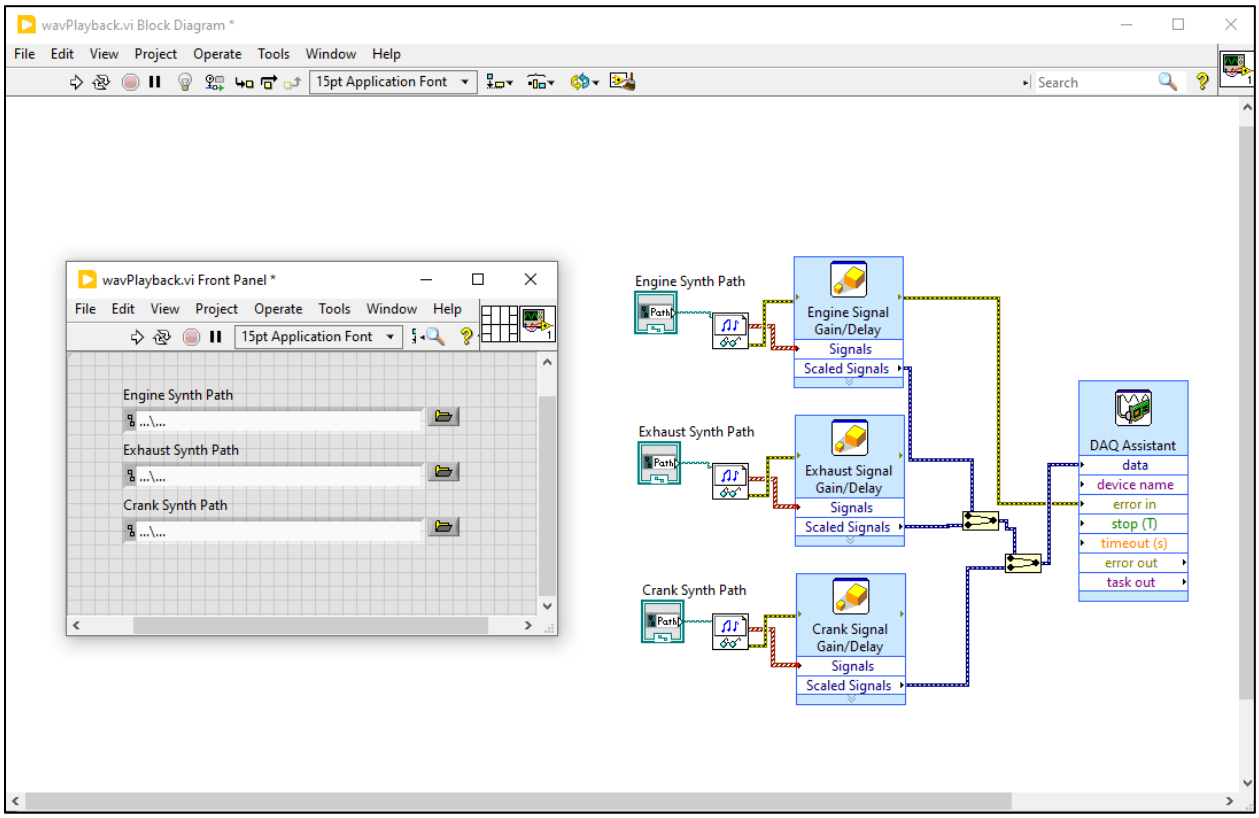

Figure 3-11: Overview of both LabView windows. The smaller window manages the .wav file path searching and the signal flow with accompanying gain/delay blocks is shown to the right.

The primary noise playback speakers used in this study undoubtedly modify the noise with their own frequency response. Therefore, it is desired to use speakers with a frequency response as flat as possible in the frequency range of interest. For this study, “JBL EON ONE” speakers were selected due to being self-powered speakers with good power overhead and a relatively flat low frequency response due to the presence of a ten-inch diameter subwoofer. That being said, it ultimately only matters that the system is capable of reliably playing back the frequency content that is necessary to provide a target for cancellation. In essence, the frequency response of the speakers becomes a portion of the primary path and does not detract from system performance or introduce error.

3.7 ANC Demonstration Hardware Integration

The ANC system hardware comes in the form of two modules with their accompanying wire harnesses for making the various necessary electrical connections. The first module is primarily a microcontroller (MCU) and digital signal processor (DSP) chip which are responsible for signal routing and operating the FxLMS algorithm. The second acts as a digital to analog converter (DAC) and signal amplifier to provide speaker level anti-noise signals which are played through the JBL EON ONE speakers. For the remainder of this thesis, the first module will be referred to as the control module and the other will be referred to as the booster amplifier which together for the ANC demonstration hardware.

The control module performs the RPM calculation and therefore requires wiring the crank signal to an available PWM channel. The control microphones are then connected and routed via the tuning software to the inputs of the FxLMS tuning block. The anti-noise outputs from the block are then routed to the digital audio outputs which are connected to the booster amplifier. Finally, the control module must be switched into an active power state via a CAN message which is provided via a USB CAN controller and software on the test operator's computer. The booster amplifier then uses the digital input connections to convert, route and amplify the anti-noise signals to the various speaker output channels. Because only one control speaker is used in the study, only one control channel needs to be connected.

With all the necessary physical connection made on the ANC demo hardware, the first measurements of the enclosure and ANC system may begin. The control module is flashed with reference code for narrowband FxLMS and an initial set of generic tuning parameters is loaded. The final step in making the system fully functional is the measurement of an impulse response which is handled via an onboard protocol based on Farina's ESS method. While keeping the test

environment as quiet as possible, the ANC system measures and stores all the speaker and microphone secondary path estimations measured this way and they may each be exported for analysis. For this research, the ESS chirp ranges from 10 to 650 Hz over 0.5 seconds and the response is sampled at 1.5KHz. 250 taps were then used for the FIR. All results shown in Chapter 4 are compared using 1024 spectral lines.

It is noted that the FEA model will likely have lower magnitude low frequency performance than this measured impulse response due to the not being able to perform an exponential frequency step in a frequency domain simulation. The ANC system will therefore input more low frequency energy over the test duration than the FEA model predicts but this comes at the benefit of not requiring a time domain FEA model which is computational much more taxing. This will be discussed more in the relevant latter section.

3.8 ANC System Performance Measurement

Following these procedures, the test environment is prepared and engine noise may then be attenuated in the enclosure using the integrated ANC system. To record the results, each random incidence measurement microphone is connected to an input channel of the Squadriga II and a split from the ANC system crank signal is connected to a pulse channel of the front-end so that results may be analyzed versus RPM or as order cuts. Since all primary noise files are of a known duration, start and end triggering may be done very consistently by configuring the recording to start on a pressure level increase on any of the enclosure microphones and stopping after the requisite recording duration is collected.

Since this process is highly repeatable, modifications to the primary noise loaded in LabView or to the FxLMS system tuning parameters may be made and then the system behavior may be

recorded once again. By turning the anti-noise generation off, one may gather a system baseline against which all parameter modifications may be compared. Using this method, the FxLMS parameters were then modified and evaluated iteratively until the maximum level of SPL reduction was achieved. From inspection of the filter update equation, it can be seen that a nominal range for the μ term must be determined based on the magnitude of the secondary path estimations as well as the error signals. A leakage term (ν) slightly below one (on the order 0.99) allows for filter growth but greatly aids in system stability. This system tuning was then saved and labeled as the optimized tuning file which would be used for all future comparisons between the measured and modeled secondary path estimations.

Chapter 4: Results Analysis

Presented here are the results of data collection and analysis discussed in the previous chapters. An overview of the various modeling changes made to approach an acceptably low level of variance between the measured and simulated secondary path estimations is discussed and ultimately the study concludes with the quantitative and qualitative analysis of the final ANC system performance estimation. For the benefit of the reader, it is also worthwhile noting that this chapter will review large amounts of data and therefore all figures will be presented at the end of the chapter.

4.1 IR Data Comparisons

Each impulse response comparison figure includes twelve plots. They are all organized consistently where the first row displays the time domain response, the second row displays the magnitude response, and the third row displays the phase response. The columns are organized by microphone-to-speaker pairs and are done so in order. Therefore, the first column is the time, magnitude and phase response of the control loudspeaker to the first control microphone at position "MIC 2" (reference Table 3-1 as necessary). The second column refers to these same relationships for the control loudspeaker to the second control microphone at position "MIC 3" and so on.

When qualitatively analyzing these plots, it is critical to keep the following metrics in mind:

- The first arrival of energy in each time domain plot should be identical. This takes the form of the alignment of the first peaks in the time domain response and indicates that the time

of flight and other factors that affect system delay are accounted for. If an ANC system is known to contribute additional signal delay that is significant it should be added as delay during the post-processing steps.

- The magnitude response should show a very similar overall level at all points in the frequency range of interest. This indicates that microphone and loudspeaker sensitivity were appropriately accounted for. Error in this response lowers the maximum possible achievable SPL attenuation of the ANC system.
- The phase response should similarly have a group delay that is consistent between impulse responses and be in phase with one another. Improper phase response information is possibly the most detrimental element to a functioning ANC system. This is due to the fact that once phase response error hits a critical threshold (observed to be approximately 60 degrees), the system risks not only reinforcing noise but causing the filter adaption to become divergent. This causes the systems output to increase unceasingly until it reaches safety thresholds and can rarely be overcome once started without additional system logic being utilized.

4.1.1 Acoustic vs Vibro-Acoustic Modeling Differences

Using only the acoustic model, the first impulse response was simulated and post-processed for an initial qualitative analysis (Figure 4-1). In this result, the overall shape of each response for each microphone location seems roughly appropriate. However, after further scrutiny, a few key concerns may be noted.

The time domain response of the simulated system initially looks incredibly close to the measured version. After the 0.04 second mark, the signals diverge somewhat and continue this trend to the

end of the sampling period. This series of plots did however confirm that the calculation for time of flight and accounting for system delay was appropriate since the time of arrival of the first peaks overlap well. When considering the set of magnitude response curves, one can see that there is a large difference in the characteristics of the response at low frequencies. The simulated response of the acoustic model does not feature several prominent resonances and anti-resonances. When comparing the frequencies at which these missing resonances occur with the analytical model for acoustic modes of a rectangular enclosure (refer to Table 3-2), it may be seen that they occur at frequencies below the lowest predicted acoustic mode. A simple tap test was then performed near the center of each face of the enclosure with a tri-axial accelerometer placed next to the control speaker (Figure 4-2). The analysis of these results reveals that the resonances are due to the mechanical coupling between the control speaker and the enclosure wall. The previous assumption that the stiffening of the cabin was adequate to treat the entire enclosure as infinitely rigid was therefore proven to be inaccurate and the development of a more complete vibro-acoustic model was necessary.

In parallel to creating the new vibro-acoustic model, the simulated impulse response was prepared and loaded into the ANC system to see what relative amount of estimation accuracy it could achieve. Because of the positive notes mentioned earlier and the additional fact that the phase response appeared to be consistent with the measured impulse response below 200Hz, it was not a foregone conclusion yet that the system would respond inappropriately. However, with the inaccuracies of the model at that stage, the ANC system behavior during testing was divergent. The anti-noise output quickly increased to the safety thresholds put in place and remained there for the duration of the surrogate primary noise testing (Figure 4-3).

With such a negative primary result, all assumptions were reevaluated. Ultimately, it was determined that the majority of the initial assumptions remained valid, however, an extra round of results analysis was deemed worthwhile and is explored in the next section.

The impulse response comparison from the vibro-acoustic model was then compared to the measured result (Figure 4-4). Of primary importance is noting the corrected characteristics of the magnitude response curves. The vibro-acoustic model does underestimate the level of magnitude response curves at lower frequencies; however, this is to be somewhat expected given that the frequency domain FEA model is not using an ESS as the Farina method prescribes and therefore there is less low frequency energy input to the system. The new impulse response dataset shares many of the other same positive characteristics of the first result. The arrival time for energy in the time domain model remains accurate and the phase response appears to not be significantly better or worse than the result from the acoustic model. The introduction of the coupling with the structure did add considerable reverberation of 140Hz content which is easily noticed in both the time domain and frequency domain plots. This 140Hz resonance does appear in the tap testing but seems more pronounced than one would expect given the relative size of that peak from the tap testing. Furthermore, the vibro-acoustic model introduced a size-able DC offset to the signal that was not previously present, but this was largely filtered out due to the post-processing recommendations from Farina.

4.1.2 Impacts of Various Post Processing Methods

Additionally, post processing was considered and tested as a part of this study. The previous comments regarding the introduction of a sizeable DC component from the vibro-acoustic model are worth reintroducing here. From the magnitude response curves in the vibro-acoustic model's

impulse response dataset, a low frequency resonance that does not exist in the measured set of curves can be seen. If the Farina post processing is removed, it may be seen that this energy is simply the unfiltered portion of the DC offset.

Several experiments where ran with various augmentations to the critical frequencies of Farina's prescribed methods and then several more were ran in addition where simple high and low pass filtering was applied at various frequencies (around 500-600 and 10-30 respectively) to attempt to gain insight on how this would impact final system performance estimation. However, the results from these experiments were trivial. The impact of any of these modifications on the predicted behavior was so small as to be considered de minimis.

4.2 ANC System Performance Analysis

By comparison with the previous generation's results, the final ANC system performance results using the impulse response dataset from the vibro-acoustic model were incredible. Not only did the anti-noise filter adaptation remain convergent at all operating frequencies tested but the system behavior was consistent with that which was seen while using the measured impulse response. Put more plainly, that is to say that if the ANC system was attenuating or reinforcing content at a given frequency then it was doing so with both the measured and simulated impulse responses. Presented here is a table of the steady state A-weighted SPL at all microphone locations during the experiments which used the synthesized primary noise and crank signals (Table 4-1).

The only instances in which the model did not accurately predict attenuation or reinforcement were at a high RPM value and in two microphone locations. However, an important qualification to that remark must be made in that - in these instances - there were essentially no differences between the estimated and actual values. In each instance, highlighted in red, the error between the

measured and estimated levels is less than two tenths of a decibel which is not perceivable and functionally meaningless. Meanwhile, percent error between the estimated and actual system performance was incredibly low at no higher than one percent which in that particular instance amounted to 0.74dB. This trend continues when focus is instead placed on the surrogate primary noise data (Figure 4-5). Presented here is an A-weighted level versus time 4th engine order cut for each microphone location. The reader may find it beneficial to refer to the RPM trace of this data to reacquaint with the vehicle state over the duration (Figure 3-10).

Table 4-1: Single values table of steady state SPL (A-weighted) for all microphone locations using the synthesized primary noise and crank signals (constant RPM for 30 seconds).

600 RPM	**MIC 1**	**MIC 2**	**MIC 3**	**MIC 4**	**MIC 5**	**MIC 6**	**MIC 7**
ANC Off [dB(A)]	60.20	61.09	61.00	60.01	61.19	58.52	60.24
Meas. ANC On [dB(A)]	57.25	57.97	58.03	57.07	58.31	56.56	58.58
Sim. ANC On [dB(A)]	57.38	58.12	58.19	57.23	58.47	56.74	58.76
SPL Attenuation [dB(A)]	2.95	3.12	2.97	2.94	2.88	1.96	1.66
% Error	0.23%	0.26%	0.28%	0.28%	0.27%	0.32%	0.31%
1200 RPM	**MIC 1**	**MIC 2**	**MIC 3**	**MIC 4**	**MIC 5**	**MIC 6**	**MIC 7**
ANC Off [dB(A)]	78.95	77.57	78.69	75.44	76.86	76.84	78.53
Meas. ANC On [dB(A)]	76.97	75.66	76.78	73.78	75.20	77.70	79.56
Sim. ANC On [dB(A)]	76.84	75.01	76.50	73.04	74.54	77.94	79.74
SPL Attenuation [dB(A)]	1.98	1.91	1.91	1.66	1.66	-0.86	-1.03
% Error	-0.17%	-0.86%	-0.36%	-1.00%	-0.88%	0.31%	0.23%
1800 RPM	**MIC 1**	**MIC 2**	**MIC 3**	**MIC 4**	**MIC 5**	**MIC 6**	**MIC 7**
ANC Off [dB(A)]	76.94	80.55	80.13	78.73	79.86	77.51	79.53
Meas. ANC On [dB(A)]	77.26	80.93	79.98	78.75	79.70	75.14	77.02
Sim. ANC On [dB(A)]	77.43	81.06	80.19	78.93	79.92	75.68	77.63
SPL Attenuation [dB(A)]	-0.32	-0.38	0.15	-0.02	0.16	2.37	2.51
% Error	0.22%	0.16%	0.26%	0.23%	0.28%	0.72%	0.79%

Just as with the synthesized primary noise and crank signal data, the prediction provided is highly consistent when depicting the measured system's behavior. There exists a few points of interest where the simulated impulse response system shows little to no performance when the actual system did in fact attenuate or reinforce the noise (for example: "MIC2" or "MIC6" at approximately 50 seconds). However, overall, the prediction is accurate and never incorrectly stating that the system is attenuating when the measured system is reinforcing noise or vice versa.

When considering the relative levels of both “ANC On” curves, an average range of around two to four decibels of prediction underperformance is noted. Given the remaining error between the measured and modeled impulse responses, this outcome is to be expected. It is understood that error between the secondary path estimation and the actual acoustic secondary path has the effect of placing limits on FxLMS ANC system performance. This may be seen in the data at idle speeds but also after the first ramp up at approximately 45 seconds in the “MIC6” and “MIC7” positions. It seems to occur equally when predicting both attenuation and reinforcement. Additional potential future improvements to this method are discussed in the following chapter.

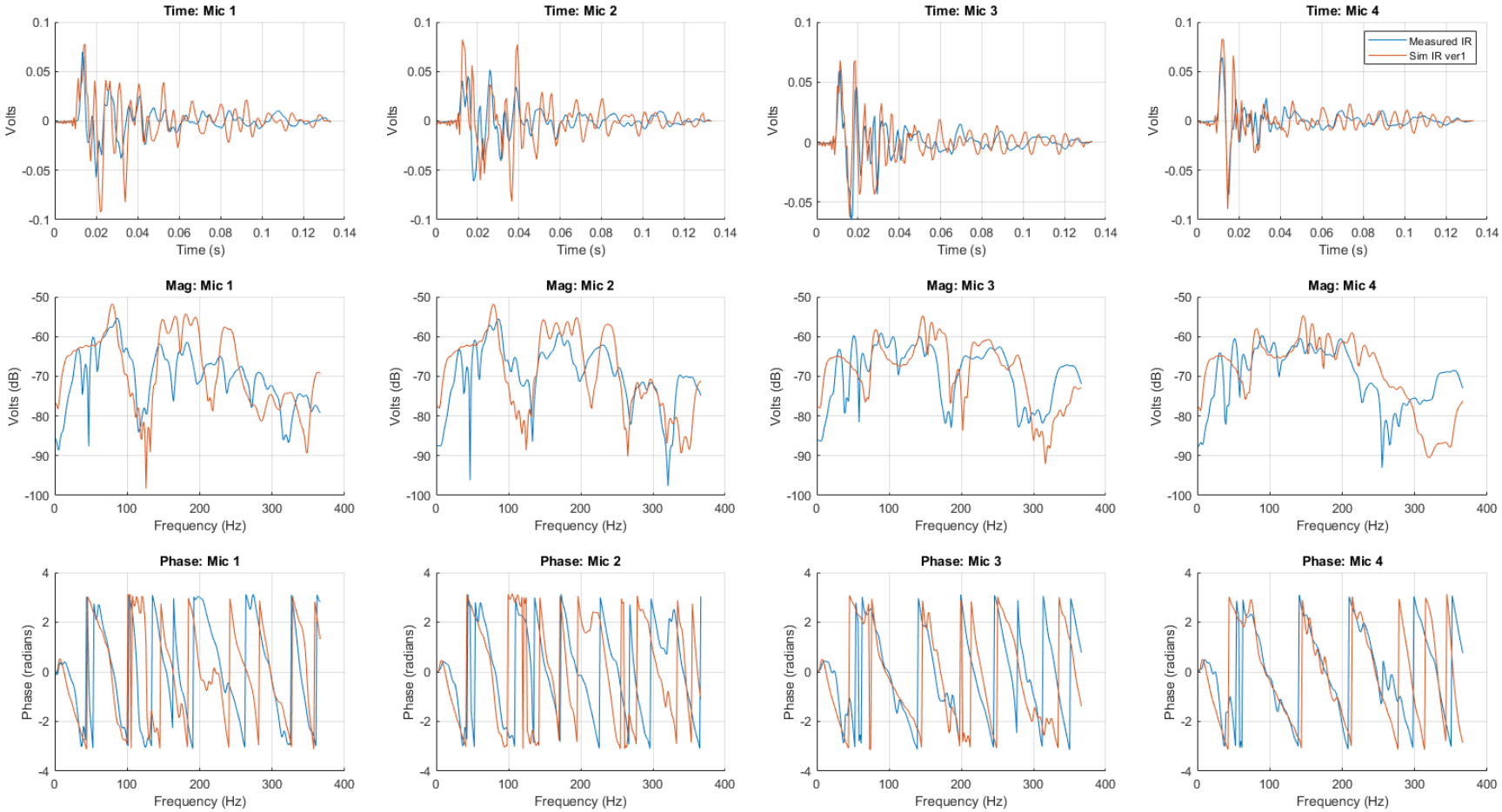

Figure 4-1: Impulse response plot which shows an overlay of the measured (blue) and simulated (orange) datasets. The simulation dataset here is from an acoustic model and does not simulate mechanical coupling. An ideal result is curves overlapping. The legend in the top right plot applies to all plots in this figure.

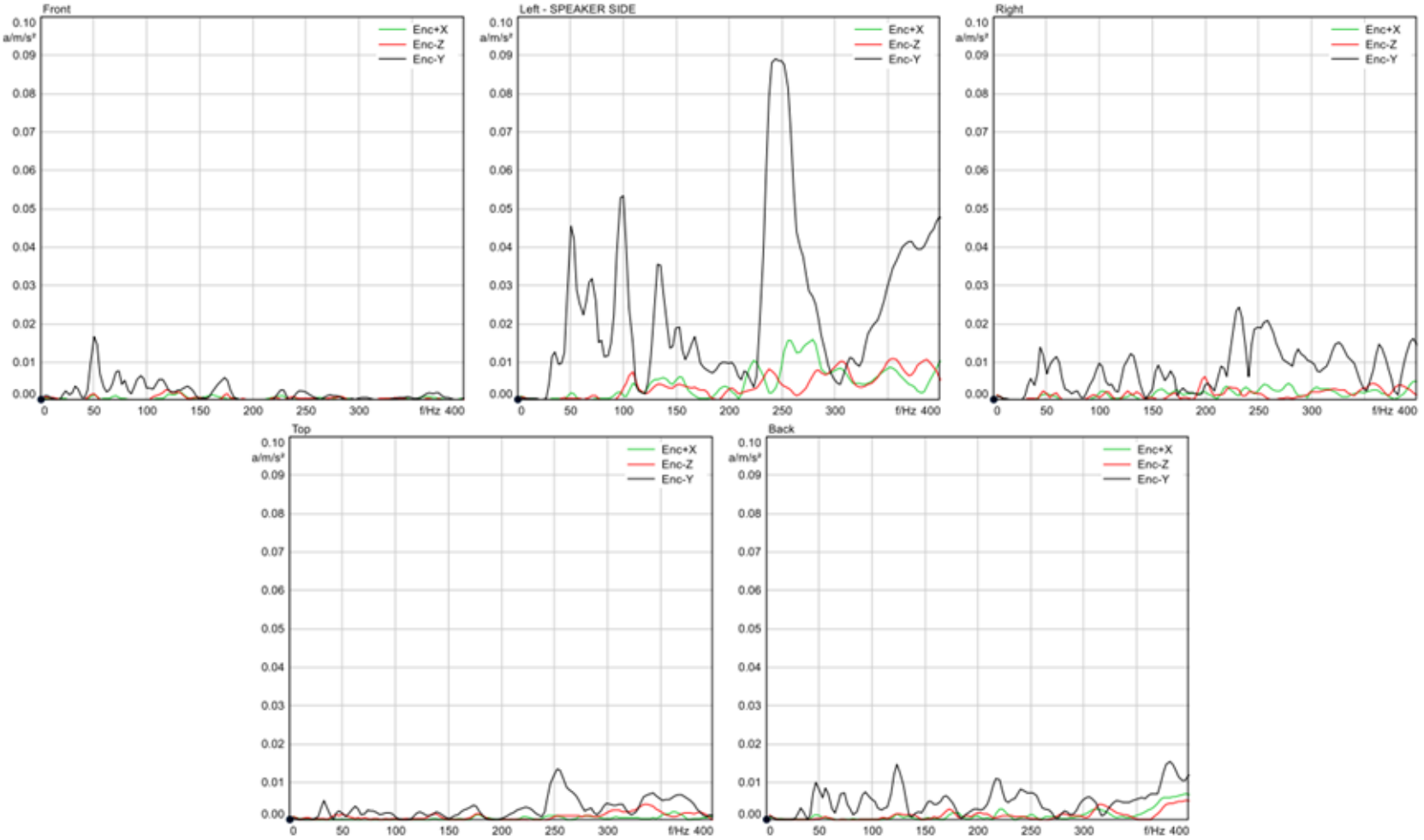

Figure 4-2: Results from impact testing displayed in the frequency domain. The "Left - SPEAKER SIDE" plot clearly shows the resonances missing from the acoustic model's secondary path estimation.

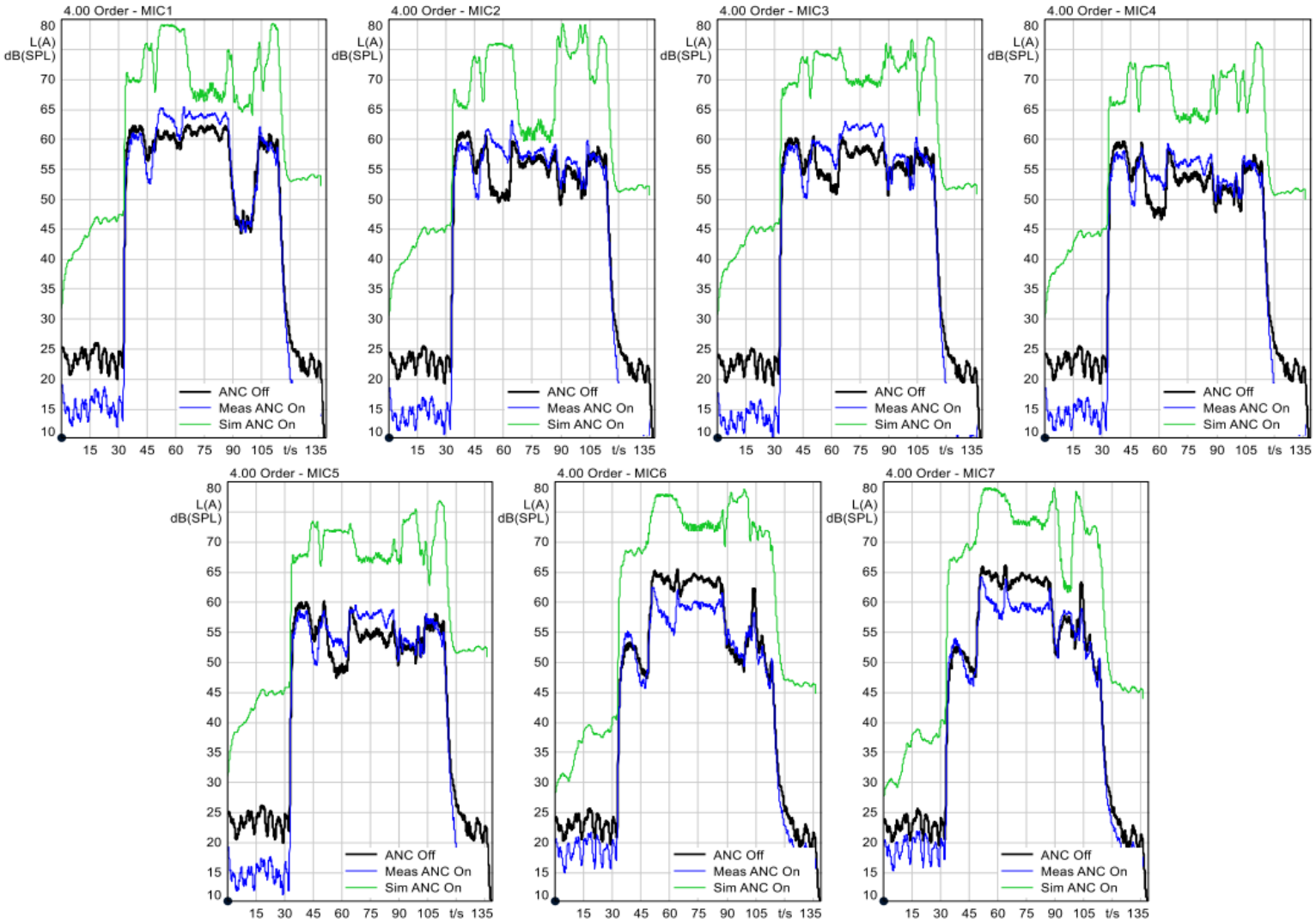

Figure 4-3: Fourth engine order noise levels in the enclosure at all microphone positions. Plots all show the divergent behavior before the estimation improvements of the mixed physics model were realized. All plots are an overlay of the system without active control or "ANC Off" (black), active control on using the measured impulse response "Meas ANC On" (blue) and active control on using the simulated impulse response “Sim ANC On” (green). The ideal result is that the green curve completely overlaps the blue curve.

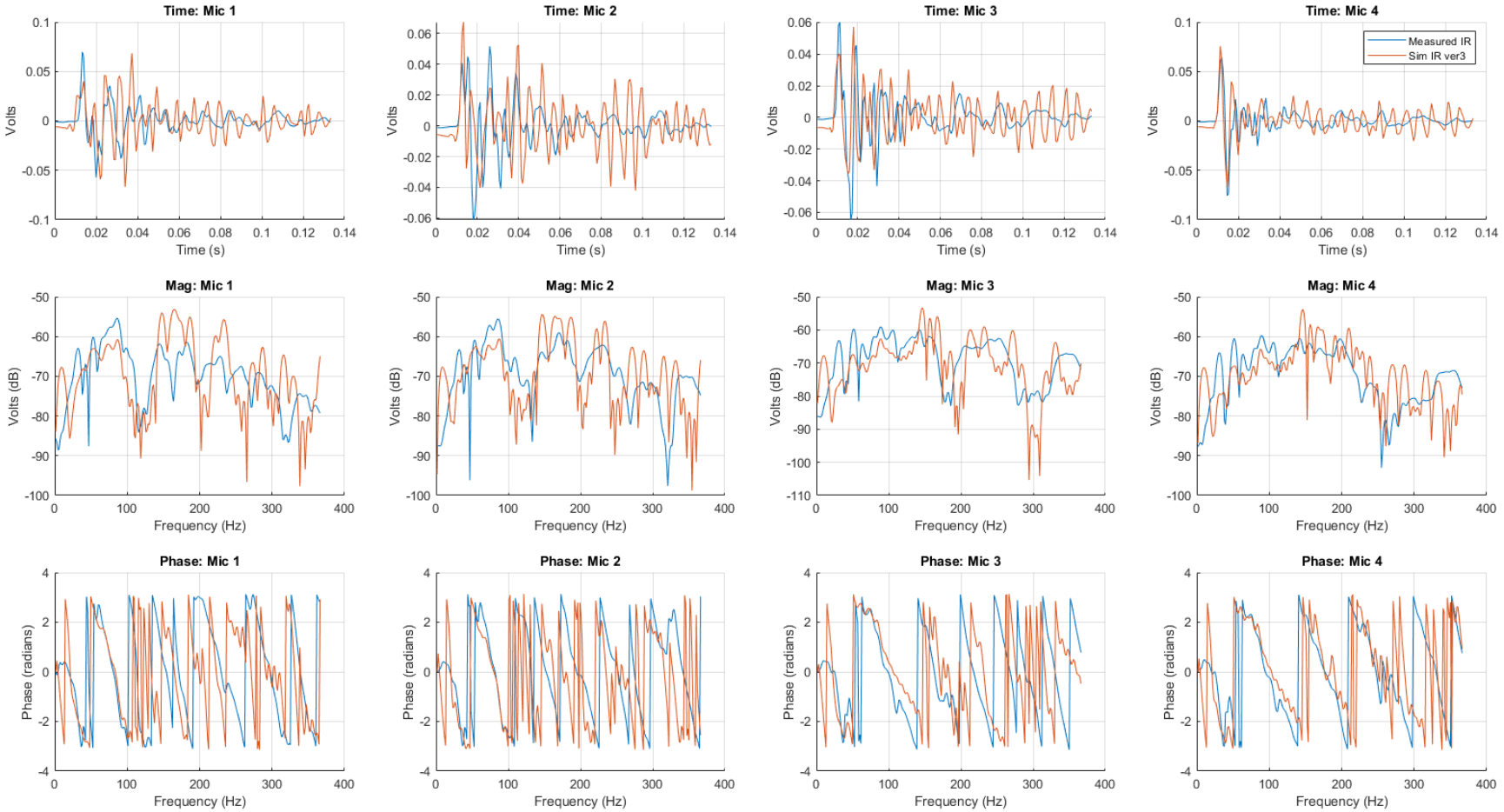

Figure 4-4: Impulse response plot which shows an overlay of the measured (blue) and simulated (orange) datasets. The simulation dataset here is from a mixed physics vibro-acoustic model and therefore simulates mechanical coupling between the control speaker and enclosure wall.

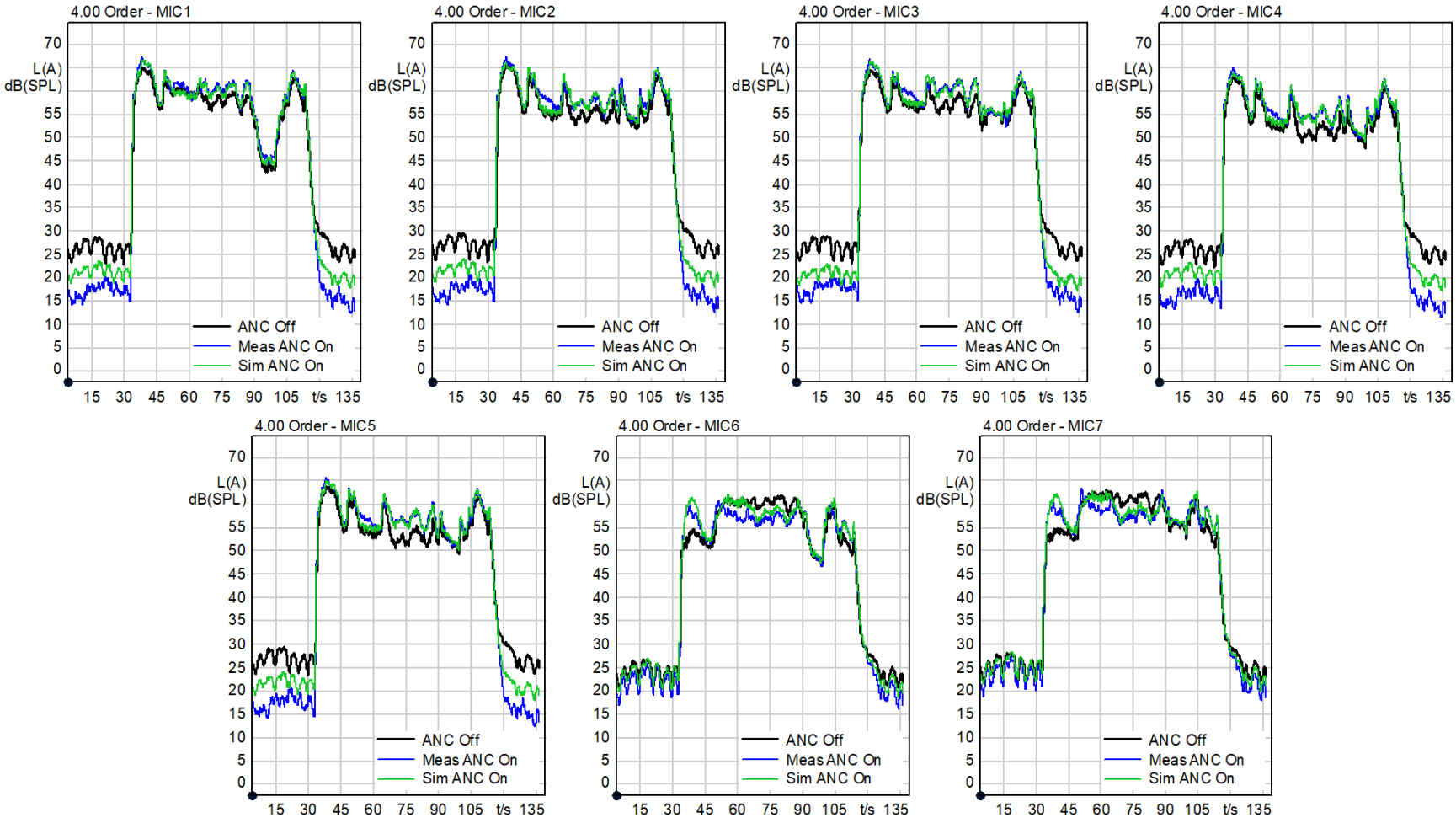

Figure 4-5: Fourth engine order noise levels in the enclosure at all microphone positions. All plots are an overlay of the system without active control or "ANC Off" (black), active control on using the measured impulse response "Meas ANC On" (blue) and active control on using the simulated impulse response “Sim ANC On” (green). The ideal result is that the green curve overlaps with the blue curve completely.

Chapter 5: Conclusions and Recommendations

Through the modifications of some of the original assumptions made, it has been shown that this method for creating a predictive model can reproduce critical system behaviors of the FxLMS ANC system. At the outset of this thesis, several key factors for success were identified:

- Fully account for the transducers of the ANC system in the model

  Through the implementation of the LPM method within the FEA model, one is able to quickly adjust control speaker parameters based on information readily available to system integrators and OEMs. In parallel, assuming that the control microphones have a relatively flat response in the ANC system operating frequency range allows the operator to use a pre-determined scaling factor for the magnitude of the simulated system response that is determined by microphone sensitivity. This means that all control transducers are fully incorporated into the model.

- Allow for adjustment of the primary path to simulate the addition or removal of passive NVH enablers

  Similar to the processes described by Stanef and Khatokar *et al.*, this process allows the primary noise to first be filtered offline through convolution with a simulated primary path. While this thesis' testing does not require this process to be used, it remains a commonly accepted method for applying any primary path to a noise signal which further aids the operator in assessing various planned environments.

- Allow for the modification of the input signal to accommodate changes in the powertrain design or use of synthesized content

    Via the methods of surrogate or synthesized noise, this model has shown to properly predict system behavior. So long as an appropriate sync pulse is provided with any recording of noise, this information can be input to a SIL or HIL test environment and tested as described in this thesis.

- FxLMS tuning parameters should be easily modifiable to enable the system to be optimized quickly, thereby mimicking the vehicle tuning processes and making them more natural for engineers to engage with

    By using a HIL environment specifically during this testing, operator interface with the tuning software and amplifier is made even more simple than interfacing with it installed in a vehicle. Furthermore, due to the simple fact that the actual system hardware is operating as if it were in a vehicle environment, there is no additional operator training required if they are already familiar with the tools and tuning processes.

- Algorithmic behavior should be properly accounted for and modifiable to allow for carryover of this process to future ANC systems (new features, new algorithms, etc)

    Once again, because of the implementation with SIL and HIL testing environments, reference code and even production samples may be evaluated with all intended system behavior and features reflected in the results. So long as the system requires the use of a secondary path estimation this process remains valid for use.

- The computational cost to operate should be kept as low as possible while still achieving SPL reduction estimates that are appropriate; thereby allowing for rapid iterations

    Of all of the pre-identified key performance indicators (KPIs), this was always likely to be difficult to obtain without further qualification. As previously mentioned, the resulting predictive model was nearly completely consistent with the reference system when projecting whether attenuation or reinforcement of noise content would occur at a given frequency for any given primary noise. However, the fact remains that averaging a two to four decibel offset between prediction and reference systems when attenuation or reinforcement reaches larger values reflects a level of error that trained listeners could perceive. There are further methods that may be employed to continue to lessen this error, however, they do require a substantial increase in computational cost which turns this KPI into a trade-off. Like many other facets in systems engineering, trade-offs like this are not unacceptable but they do require more precision, forethought and training and this is likely an area to improve greatly as experiential learning and computational power continue to grow in this area. Thoughts for future improvement to accuracy and extended applications are therefore presented in the following sections.

5.1 Potential Simulation Improvements via Time Domain Model

One of the last items discussed as a part of the testing phase of this research was whether to shift the vibro-acoustic model from the frequency domain to the time domain. Primarily, this was seen as a simple step to close a known gap in the measurement process of the secondary path estimations. As previously stated, the Farina method prescribes an ESS chirp which cannot

properly be reflected in the frequency domain model. This is thought to likely contribute to the low frequency magnitude response error where one may note that the simulated impulse response has a significantly lower level. Due to the nature of narrowband FxLMS ANC systems being intended on low frequency noise content, this improvement is an interesting first target for future increases in accuracy.

After further consideration however, it was determined that pursuing this approach would likely not be appropriate in this study. Firstly, shifting the model into the time domain would require a considerable increase in computational complexity which is not in line with the corresponding KPI. It was determined that in a majority of automotive applications the level of error seen here would not be detrimental to overall project success. Since all ANC implementations would still see a real-world pre-production tuning iteration this error must therefore be compared with the level of change seen between build stages. Past experience dictates that these values are roughly equivalent in most instances. As a continuation of this study in particular, the increased computational time is hard to justify when, instead, a project partnership with an OEM could instead be developed reducing error in many other areas simultaneously.

5.2 Future Partnered Projects with OEMs

This section further expands on the value of shifting towards a partnered project with an OEM as alluded to in the previous section. Given the further confidence in developing a high-quality model from the work presented in this thesis, chances of project success are high and an opportunity exists to become a solution provider in advance of a hard shift to the aforementioned “Design Right First” principles.

5.2.1 OEM Originated CAD Models

An obvious challenge for this thesis was minimizing the research and labor effort on creating an accurate model since this area of study is already well established. This limited the scale to a simple wooden enclosure given the desire to see results validated against actual hardware in an identical situation. However, a partnered research project with an OEM would immediately lift this restriction. OEMs have for many years created highly accurate CAD models which could be used for this continued study. Especially given that audio system suppliers already are tasked with providing CAE analysis for auralizations, conducting this type of work on these models is a natural extension of their capabilities. Moving towards using these detailed models introduces additional complexity, however, this can be somewhat offset by having access to historical datasets of similar vehicle designs which are validated once prototypes do exist.

5.2.2 Improved Mechanical Properties Stability

Helping to further offset the complexity of an actual vehicle enclosure is the increase to mechanical property stability of the design materials. For ease of manufacturing, the enclosure was created from and stiffened with entirely wood products. OSB and pine 2x4 studs are easy to work with but their mechanical properties vary far more than metals. This presented an extra challenge when shifting to the vibro-acoustic model since material property libraries could not be relied upon for a high level of accuracy. Even day-to-day changes in humidity effected the density and dimensions of the enclosure's components since it would need to be tested in the outdoors. Simply shifting to a more stable material would help to reduce error. This also comes with the fringe benefit that the increased stiffness would help to increase the resonances of the control speaker mounts to higher

frequencies. Potentially, this could even push them out of the range of interest for these systems and remove the need for mechanical coupling to be a key consideration.

5.2.3 Upgrading to MIMO Control System Architecture

To avoid additionally introducing the effects of speaker coupling into this study and keep data handling to a minimum, only one control speaker was used. In practice, even many low cost narrowband ANC systems use all four door woofers or the front doors and some other rearward channels. This would increase the potential for ANC system attenuation levels and help control against reinforcement at various frequencies in the test data which brings the completed analysis more aligned with standard production system results. Furthermore, the increase in system noise attenuation levels gives a wider margin over which the discrepancy between measured and estimated results may be compared.

5.2.4 Validation in Real-Time Environment

An important limitation to this research is that, while it can be validated using system performance comparisons it cannot do anything more. A simulated secondary path estimation from a complete car model could not only be validated against the actual system performance but could be extended to a veritable gauntlet of tests ensuring system performance across many use cases. In reality, a vehicle's actual acoustic secondary path is constantly changing and there are often high energy disturbance signals introduced to the cabin. By treating the vehicle environment like a HIL, the simulated impulse response could be uploaded to the ANC control module in the place of the measured system and tested against vehicle loading, doors and windows opening and closing, simultaneous entertainment audio playback and many other scenarios. This information would

further assist operator's and researchers with understanding the difference in system sensitivity to these various introductions of error and qualitatively demonstrate resiliency.

5.3 Road Noise Control Applications

It is not a far leap from narrowband to broadband FxLMS applications utilizing this method. As can be seen back in Figure 2-4, the basics of the control system remain unchanged and relatively minor changes to the FxLMS algorithm are needed. When the ANC system is targeting broadband low frequency rumble from road noise, this is known in the industry as road noise cancellation (RNC). First discussed by Sutton *et al.* in 1994 [16], this technology has only seen recent mass adoption in the consumer automobile industry. However, with the rise of electrified vehicles (EVs), the need for low frequency narrowband excitation is decreasing and the need for RNC is rising. This means that, extension of this predictive methodology to RNC applications becomes an important next step. Discussed here is an overview of the additional steps required and a furtherance of current RNC research state of the art.

Since RNC applications do not use a sync pulse and instead use accelerometers placed on the body and suspension of the vehicle, the use of a vibro-acoustic model is a necessity. As detailed by Herrmann *et al.* in their 2021 article [17], it is possible to achieve an approximation of the road noise at the occupant's listening position via a hybrid model using road surface elevation as the model input. In theory then, the two missing elements needed for an RNC predictive model based on this research may be acquired from one such model. By estimating the vibrational energy from the FEA model due to the interaction with a measured reference road surface at the control accelerometer locations, the RNC system input signal may be obtained. With the primary noise and FxLMS system input signal acquired, a follow-up FEA model may be calculated which

provides the acoustic secondary path estimations. As before, with this information input to a SIL or HIL, iterative changes can be made relatively quickly since they do not require rerunning the large vibro-acoustic models which determine the primary noise and input signals. At present, there remains several challenges to this method as described. The most difficult of which is to continue to further the state of the art for large and complex FEM models. The large hybrid FEA models which Herrmann *et al.* describe are highly taxing computationally and may be the primary reason why they do not report results over 100Hz which is otherwise still well within the operating range for RNC. The other main challenge is simply having access to test tracks for validation. Elevation maps of common road surfaces are not available without measuring them first-hand and the act of measuring them requires coordination with local public works office or the private owner.

5.4 Incorporation of Remote Microphone Technique

The remote microphone technique has gained increased adoption in recent years with ANC system suppliers due to offering notable system performance benefits, as can be seen in Jung *et al.'s* 2016 article [18]. The method, in short, seeks to solve the issue of control microphones not being mounted next to the occupant's ear locations by instead estimating the instantaneous acoustic signal at that location using a set of transfer functions applied to the control microphone signals. These transfer functions consist of the secondary path estimation from the control loudspeaker to each control microphone ($\hat{G}_m$), the secondary path estimation from the control loudspeaker to each remote microphone location ($\hat{G}_e$) and the linear function that estimates the noise at the remote microphone location based on the signal at each control microphone location ($\hat{O}$). Since $\hat{G}_m$ is simply the same secondary path estimations conducted during the original scope of work for this study, $\hat{G}_e$ may be modelled in an identical manner. $\hat{O}$ however, cannot be modeled this way. Even

with that being the case, with both $\hat{G}_m$ and $\hat{G}_e$ acquired, the system operator may operate the SIL or HIL test environment to generate the noise signals at each set of microphone locations which allows for the offline calculation of $\hat{O}$ exactly as described by Jung *et al.* In theory, this would therefore enable the use of the remote microphone technique with this predictive method and simply requires experimental validation.

Appendices

Appendix A: Primary Noise and Crank Signal Synthesis Script

An example MATLAB script which may be used to synthesize engine order content along with a correlated crank signal. Here example parameters are set for a V8 engine. The final output are WAV files which may be appropriately gained during playback to expected levels via a microphone for HIL models or via companion scripts for SIL models. Synthesized crank signal assumes 60-2 pulse design.

```
clear all
close all
clc

%Settings
rpm = 1000;      %engine speed in RPM

duration = 30;  %output .wav duration in seconds
fs = 2^14;     %sampling rate in Hz
fftSize = 2^14;

FreqRatioA = 4; %first engine order
gainA = 1;      %gain of first EO
FreqRatioB = 6; %second engine order
gainB = 0.1;    %gain of second EO
FreqRatioC = 8; %third engine order
gainC = 0.4;    %gain of third EO

%Initial data processing
oscAFreq = FreqRatioA*rpm/60;
oscBFreq = FreqRatioB*rpm/60;
oscCFreq = FreqRatioC*rpm/60;

t = linspace(0, duration, duration*fs);

%Oscillator creation
oscA = gainA.*sin((2*pi*oscAFreq).*t);
oscB = gainB.*sin((2*pi*oscBFreq).*t);
oscC = gainC.*sin((2*pi*oscCFreq).*t);

signal = oscA + oscB + oscC;

%RPM signal creation
%-> Angular velocity setup
```

```
angV = 360*rpm/60;
crnkPhase = angV.*t;
crnkPhase = mod(crnkPhase, 360);

%-> Hall effect replication
crankLogic = crnkPhase;
crankLogic(crankLogic > 345) = 359;
crankLogic = mod(crankLogic, 360/120*2);
crankLogic = (crankLogic - 3)*-1;
crankLogic(crankLogic <= 0) = 0;
crankLogic(crankLogic > 0) = 1;

%.wav writing
EngSignal = 0.7.*signal;
ExhSignal = 0.4.*signal;
crankLogic = 0.9.*crankLogic;

audiowrite('CAESim_SynthEngine.wav', EngSignal, fs);
audiowrite('CAESim_SynthExhaust.wav', ExhSignal, fs);
audiowrite('CAESim_CrankSignal.wav', crankLogic, fs);

%Analysis
complex = fft(signal, fftSize);
mag = abs(complex);
mag = mag(1:end/2);
mag = 2.*mag;
mag = mag2db(mag);
mag = mag.';
xfreq = 0:(fs/fftSize):(duration*fs);
xfreq = xfreq.';
plot(xfreq(1:size(mag)), mag);
xlim([0,200]);
xlabel('Frequency - Hz')
ylabel('Magnitdue - dB (ref = 1)')

figure;
strips(crankLogic(1:5000));
xlabel('Samples');
ylabel('Samples');
```

Appendix B: IR Data Preparation (Frequency Enveloping and TOF Delay Addition)

An example MATLAB script which uses a .mat file containing the imported IR simulation results to output a post-processed IR with the appropriate time of flight delay samples added, the frequency enveloping prescribed by Farina [13] and resampling to a common sampling rate used by the ANC system demonstration hardware used for the experimental validation.

```
% IR Data Preparation (Resampling and Time of Flight delay addition)

clc
clear
close all

% Load Data & Settings
data = LPM_IR;

nTaps = size(data, 1);
UpsampleTarget = 48000;
fsOriginal = round((data(2, 1) - data(1, 1))^(-1));

% Create necessary time series
Mic1Ts = timeseries(data(:,2), data(:,1));
Mic2Ts = timeseries(data(:,3), data(:,1));
Mic3Ts = timeseries(data(:,4), data(:,1));
Mic4Ts = timeseries(data(:,5), data(:,1));

% Resample to 48KHz
Mic1TsRes = resample(Mic1Ts, 0:(1/UpsampleTarget):(1/fsOriginal*nTaps));
Mic2TsRes = resample(Mic2Ts, 0:(1/UpsampleTarget):(1/fsOriginal*nTaps));
Mic3TsRes = resample(Mic3Ts, 0:(1/UpsampleTarget):(1/fsOriginal*nTaps));
Mic4TsRes = resample(Mic4Ts, 0:(1/UpsampleTarget):(1/fsOriginal*nTaps));
```

```
% Calculate time of flight number of samples (<x,y,z> in meters)
Mic1Pos = [1.638; 0.8685; 1.175];
Mic2Pos = [1.638; 0.0965; 1.175];
Mic3Pos = [0.8736; 0.6369; 1.175];
Mic4Pos = [0.8736; 0.31845; 1.175];
SPKPos = [0.3; 0.965; 0.3];

c = 343;    % Speed of sound in air (meters per second)
Mic1Dist = sqrt(((Mic1Pos(1,1)-SPKPos(1,1))^2)...
             + ((Mic1Pos(2,1)-SPKPos(2,1))^2)...
             + ((Mic1Pos(3,1)-SPKPos(3,1))^2));
Mic2Dist = sqrt(((Mic2Pos(1,1)-SPKPos(1,1))^2)...
             + ((Mic2Pos(2,1)-SPKPos(2,1))^2)...
             + ((Mic2Pos(3,1)-SPKPos(3,1))^2));
Mic3Dist = sqrt(((Mic3Pos(1,1)-SPKPos(1,1))^2)...
             + ((Mic3Pos(2,1)-SPKPos(2,1))^2)...
             + ((Mic3Pos(3,1)-SPKPos(3,1))^2));
Mic4Dist = sqrt(((Mic4Pos(1,1)-SPKPos(1,1))^2)...
             + ((Mic4Pos(2,1)-SPKPos(2,1))^2)...
             + ((Mic4Pos(3,1)-SPKPos(3,1))^2));

Mic1DelaySamples = floor((Mic1Dist/c)*UpsampleTarget);
Mic2DelaySamples = floor((Mic2Dist/c)*UpsampleTarget);
Mic3DelaySamples = floor((Mic3Dist/c)*UpsampleTarget);
Mic4DelaySamples = floor((Mic4Dist/c)*UpsampleTarget);

% Add time of flight delay
dataLength = size(Mic1TsRes.Data, 1);
appendedMic1ResData = cat(1, zeros(Mic1DelaySamples, 1), Mic1TsRes.Data);
appendedMic1ResData = appendedMic1ResData(1:dataLength, 1);
Mic1TsRes.Data = appendedMic1ResData;

appendedMic2ResData = cat(1, zeros(Mic2DelaySamples, 1), Mic2TsRes.Data);
appendedMic2ResData = appendedMic2ResData(1:dataLength, 1);
Mic2TsRes.Data = appendedMic2ResData;

appendedMic3ResData = cat(1, zeros(Mic3DelaySamples, 1), Mic3TsRes.Data);
```

```
appendedMic3ResData = appendedMic3ResData(1:dataLength, 1);
Mic3TsRes.Data = appendedMic3ResData;

appendedMic4ResData = cat(1, zeros(Mic4DelaySamples, 1), Mic4TsRes.Data);
appendedMic4ResData = appendedMic4ResData(1:dataLength, 1);
Mic4TsRes.Data = appendedMic4ResData;

% Resample to 1.5KHz
Mic1TsRes = resample(Mic1TsRes, 0:(1/1500):(1/fsOriginal*nTaps));
Mic2TsRes = resample(Mic2TsRes, 0:(1/1500):(1/fsOriginal*nTaps));
Mic3TsRes = resample(Mic3TsRes, 0:(1/1500):(1/fsOriginal*nTaps));
Mic4TsRes = resample(Mic4TsRes, 0:(1/1500):(1/fsOriginal*nTaps));

% Farina IR Shaping
fftSize = 2048;
fs = 1500;
dataLength = size(Mic1TsRes.Data, 1);

fRes = fs/fftSize;

ampWin = zeros(fftSize/2, 1);
fLow = floor(10 / fRes);
fHigh = floor(650 / fRes);
deltaF = floor(5 / fRes);
for i = 1:size(ampWin, 1)
    if i > (fLow - deltaF) && i <= (fLow + deltaF)
        ampWin(i) =  (1 / (2 * deltaF)) * (i - (fLow - deltaF));
    end
    if i > (fLow + deltaF) && i <= (fHigh - deltaF)
        ampWin(i) = 1;
    end
    if i > (fHigh -deltaF) && i <= (fHigh + deltaF)
        ampWin(i) = 1 - (1 / (2 * deltaF)) * (i - (fHigh - deltaF));
    end
end
ampWin = cat(1, ampWin, flip(ampWin));
```

```
compMic1 = fft(Mic1TsRes.Data, fftSize);
ampMic1 = abs(compMic1);
phaseMic1 = angle(compMic1);
ampMic1 = ampMic1 .* ampWin;
compMic1 = (ampMic1 .* cos(phaseMic1)) + (ampMic1 .* sin(phaseMic1))*1j;
fTimeMic1 = real(ifft(compMic1, fftSize, 1));
fTimeMic1 = fTimeMic1(1:dataLength);

compMic2 = fft(Mic2TsRes.Data, fftSize);
ampMic2 = abs(compMic2);
phaseMic2 = angle(compMic2);
ampMic2 = ampMic2 .* ampWin;
compMic2 = (ampMic2 .* cos(phaseMic2)) + (ampMic2 .* sin(phaseMic2))*1j;
fTimeMic2 = real(ifft(compMic2, fftSize, 1));
fTimeMic2 = fTimeMic2(1:dataLength);

compMic3 = fft(Mic3TsRes.Data, fftSize);
ampMic3 = abs(compMic3);
phaseMic3 = angle(compMic3);
ampMic3 = ampMic3 .* ampWin;
compMic3 = (ampMic3 .* cos(phaseMic3)) + (ampMic3 .* sin(phaseMic3))*1j;
fTimeMic3 = real(ifft(compMic3, fftSize, 1));
fTimeMic3 = fTimeMic3(1:dataLength);

compMic4 = fft(Mic4TsRes.Data, fftSize);
ampMic4 = abs(compMic4);
phaseMic4 = angle(compMic4);
ampMic4 = ampMic4 .* ampWin;
compMic4 = (ampMic4 .* cos(phaseMic4)) + (ampMic4 .* sin(phaseMic4))*1j;
fTimeMic4 = real(ifft(compMic4, fftSize, 1));
fTimeMic4 = fTimeMic4(1:dataLength);

Mic1TsRes.Data = fTimeMic1;
Mic2TsRes.Data = fTimeMic2;
Mic3TsRes.Data = fTimeMic3;
Mic4TsRes.Data = fTimeMic4;
```

```
% Output resampled (formated) .mat file
Mic1Out = Mic1TsRes.Data(1:200);
Mic2Out = Mic2TsRes.Data(1:200);
Mic3Out = Mic3TsRes.Data(1:200);
Mic4Out = Mic4TsRes.Data(1:200);

OutMatrix = cat(2, Mic1Out, Mic2Out, Mic3Out, Mic4Out)
```

Appendix C: IR Comparison Script

An example MATLAB script which plots the time, magnitude and phase responses from the impulse response data. The variable "`iRGain`" should be modified to match the necessary magnitude offset as dictated by the control microphone sensitivity. By default, this script is setup to analyze one control loudspeaker and four control microphones with 200 samples per recording at 1500Hz sampling rate.

```
% ANC System Impulse Response Comparison

close all
clear variables
clc

% Settings
% Modify as desired
nFiles = 2;          %Number of files to compare
iRGain = 2.96e-4;    %Approximate gain calibration between measured
                     % and simulated impulse responses
                     % (default: 2e-4)
fs = 1500;           %Sampling Rate (ANC module uses 1500)
T = 1/fs;            %Time Step
fftSize = 1024;      %FFT Size (ANC module uses 1024)

% Load data
% Loads measurement IR which is target for all simulated files
irData = zeros(nFiles, 200, 4);

load("ANCSimProject_MeasuredIR.mat", "tsIR");
irData(1, :, :) = tsIR;
LegendEntry{1} = 'Measured IR';

% MODIFY BELOW - Load formatted IR Data
%                  Format to the following specification, timeData(i, j):
%                              i = first 200 samples of impulse response time %
%                              data
%                             j = microphone number (control microphones are 2,
%                             3, 6, 7 - see enclosure

load("LMP_IRData_Resampled.mat", "OutMatrix");
irData(2, :, :) = OutMatrix;
LegendEntry{2} = 'Sim IR;
```

```
% load("File.mat", "variableName");
% irData(n, :, :) = variableName;
% LegendEntry{n} = 'Legend Entry';

%... continue as necessary up to value of "nFiles" in setup

% Calculation (DO NOT MODIFY)
if nFiles >= 2
   for i = 2:nFiles
       irData(i, :, :) = irData(i, :, :).*iRGain;
   end
end

irDataComplex = zeros(nFiles, fftSize, 4);
irDataMag = zeros(nFiles, fftSize, 4);
for i = 1:nFiles
    irDataComplex(i, :, :) = fft(irData(i, :, :), fftSize);
    irDataComplex(i, :, :) = irDataComplex(i, : , :);
    irDataMag(i, :, :) = abs(irDataComplex(i, :, :)./fftSize);
    irDataMag(i, :, :) = 2.*irDataMag(i, :, :);
    irDataMag(i, :, :) = mag2db(irDataMag(i, :, :));
end
irDataMag(:, 251:end, :) = [];

irDataPhase = zeros(nFiles, fftSize, 4);
for i = 1:nFiles
    irDataPhase(i, :, :) = irDataComplex(i, :, :);
    irDataPhase(i, 1, :) = 0;
    irDataPhase(i, :, :) = angle(irDataPhase(i, :, :));
end
irDataPhase(:, 251:end, :) = [];

% Plot Generation (DO NOT MODIFY)
xAxisTime = T.*(1:200);
xAxisFreq = fs.*(1:fftSize)./fftSize;
xAxisFreq = xAxisFreq(1:250);

figure('Position', [0 0 1690 1080]);
for k = 1:nFiles
    subplotIndex = 1;
    for i = 1:3
        for j = 1:4
            subplot(3, 4, subplotIndex);
            hold on
            grid on
            if i == 1
                plot(xAxisTime, irData(k, :, j));
                title(['Time: Mic ', num2str(j)])
                xlabel('Time (s)');
                ylabel('Volts');
                if k == nFiles && j == 4
                    legend(LegendEntry);
                end
            elseif i == 2
                plot(xAxisFreq, irDataMag(k, :, j));
                title(['Mag: Mic ', num2str(j)])
                xlabel('Frequency (Hz)');
```

```
                ylabel('Volts (dB)');
            elseif i == 3
                plot(xAxisFreq, irDataPhase(k, :, j));
                title(['Phase: Mic ', num2str(j)])
                xlabel('Frequency (Hz)');
                ylabel('Phase (radians)');
            end
            subplotIndex = subplotIndex + 1;
        end
    end
end
set(gcf, 'visible', 'on');
```

Appendix D: Sorted Rectangular Enclosure Acoustic Mode Search Script

An example Python script which calculates the eigenfrequencies for various acoustic modes and then sorts the output by the lowest eigenfrequencies, thereby giving a convenient expression of where resonances and anti-resonances should be detectable in the experimental results. The analytical model for this search is detailed in Chapter 3.3.

```
import numpy as np

c = 343
length = 2.184
width = 0.965
height = 1.175

class ResonantMode:
    def __init__(self, m, n, p):
        self.m = m
        self.n = n
        self.p = p

        self.eigenfrequency = self.calculate_eigenfrequency()

    def calculate_eigenfrequency(self):
        return c / (2 * np.pi) * np.sqrt(np.power(self.m * np.pi / length, 2)
+
                                         np.power(self.n * np.pi / width, 2) +
                                         np.power(self.p * np.pi / height, 2))

    def __str__(self):
        return 'eigenfrequency: {0}    m: {1}    n: {2}    p: {3}\n'.format(
            self.eigenfrequency, self.m, self.n, self.p)

    def __repr__(self):
        return str(self)


resonantModes = list()
for m in range(5):
    for n in range(5):
        for p in range(5):
            resonantMode = ResonantMode(m, n, p)
            resonantModes.append(resonantMode)


print(sorted(resonantModes, key=lambda x: x.eigenfrequency))
```

Appendix E: Enclosure Dimensions

Wooden Studs (Pine) Cross-Section:

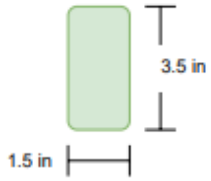

OSB Sheeting:

1/2 inch Thick
4 foot by 8 foot sheets cut to size

Acoustic Foam:

1/2 inch Thick Flat Sheet
4 foot by 8 foot sheets cut to size

Rubber Caster Wheels

Wooden Structure (Top View):

NOTE: Dimensions are to center of stud and extent of sheet material unless otherwise noted

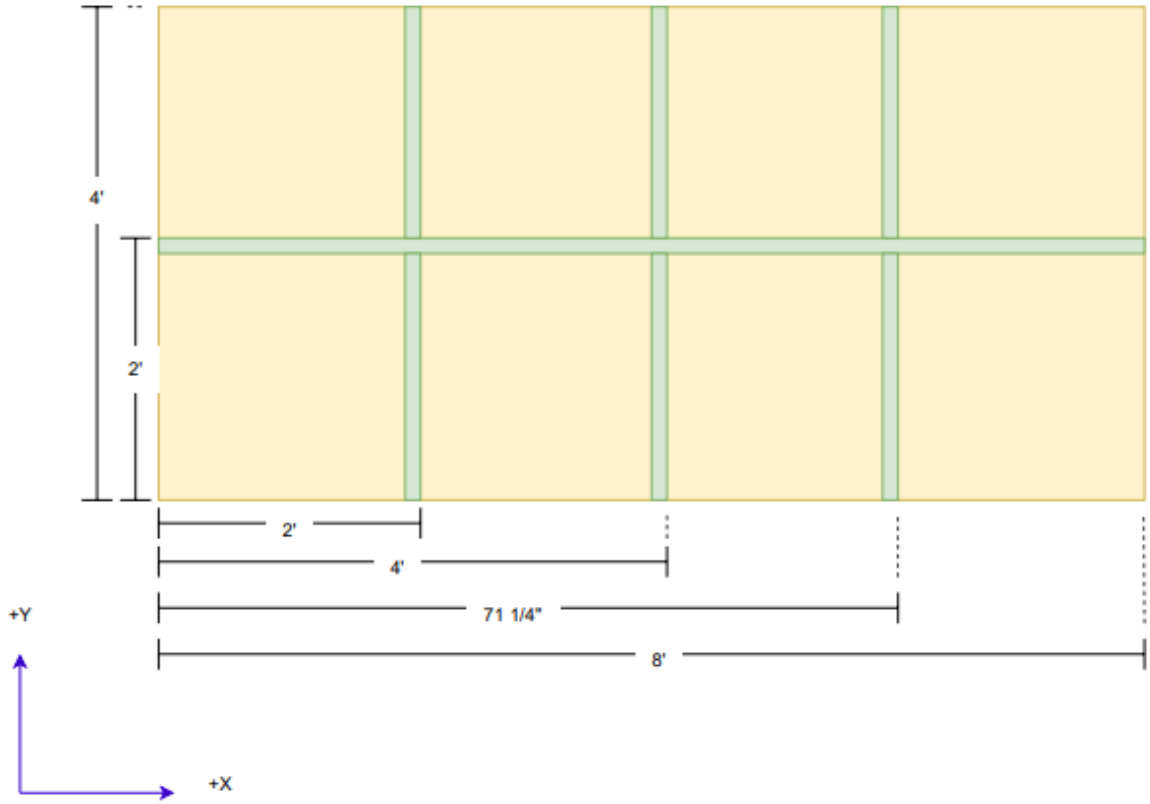

Wooden Structure (Right View):

NOTE: Dimensions are to center of stud and extent of sheet material unless otherwise noted

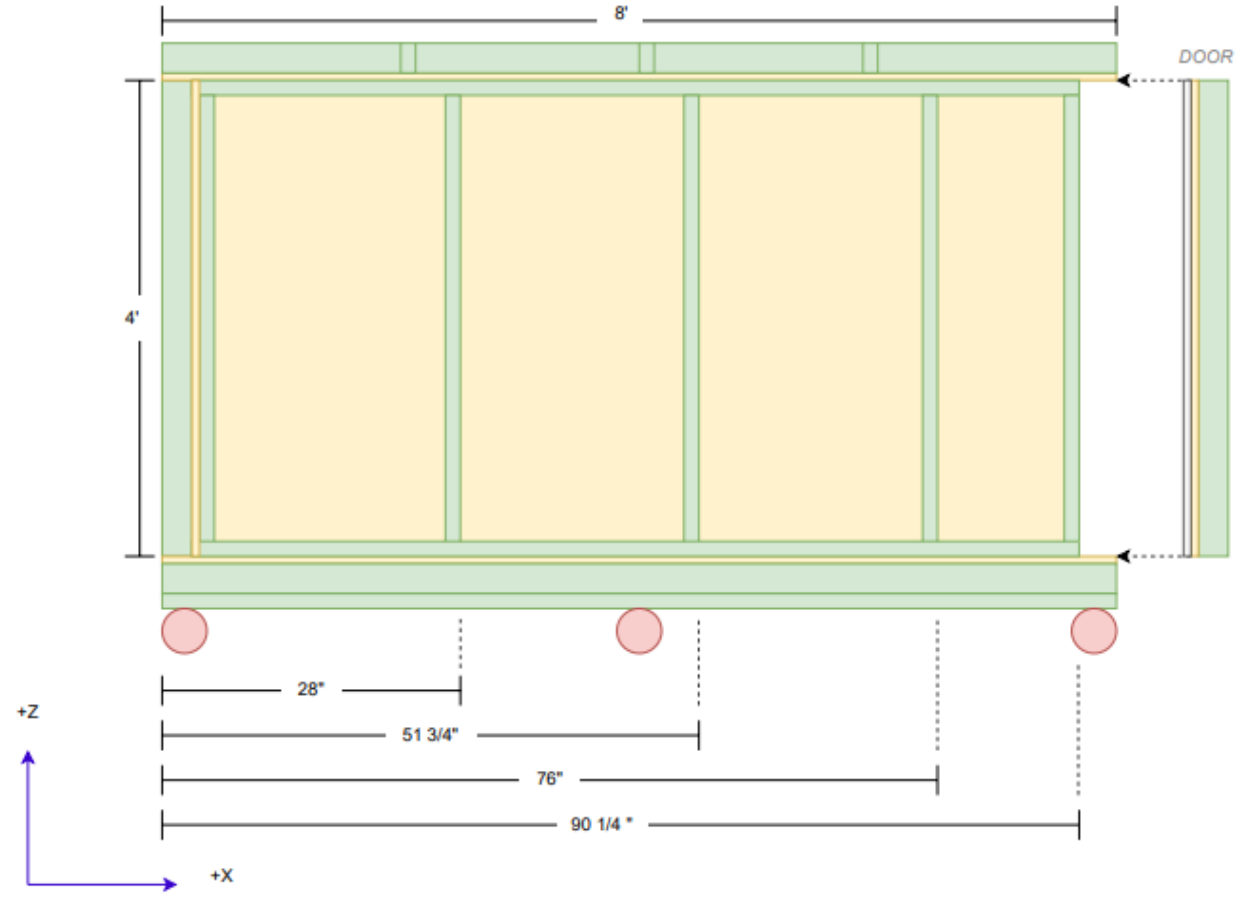

Wooden Structure (Left View):

NOTE: Dimensions are to center of stud and extent of sheet material unless otherwise noted

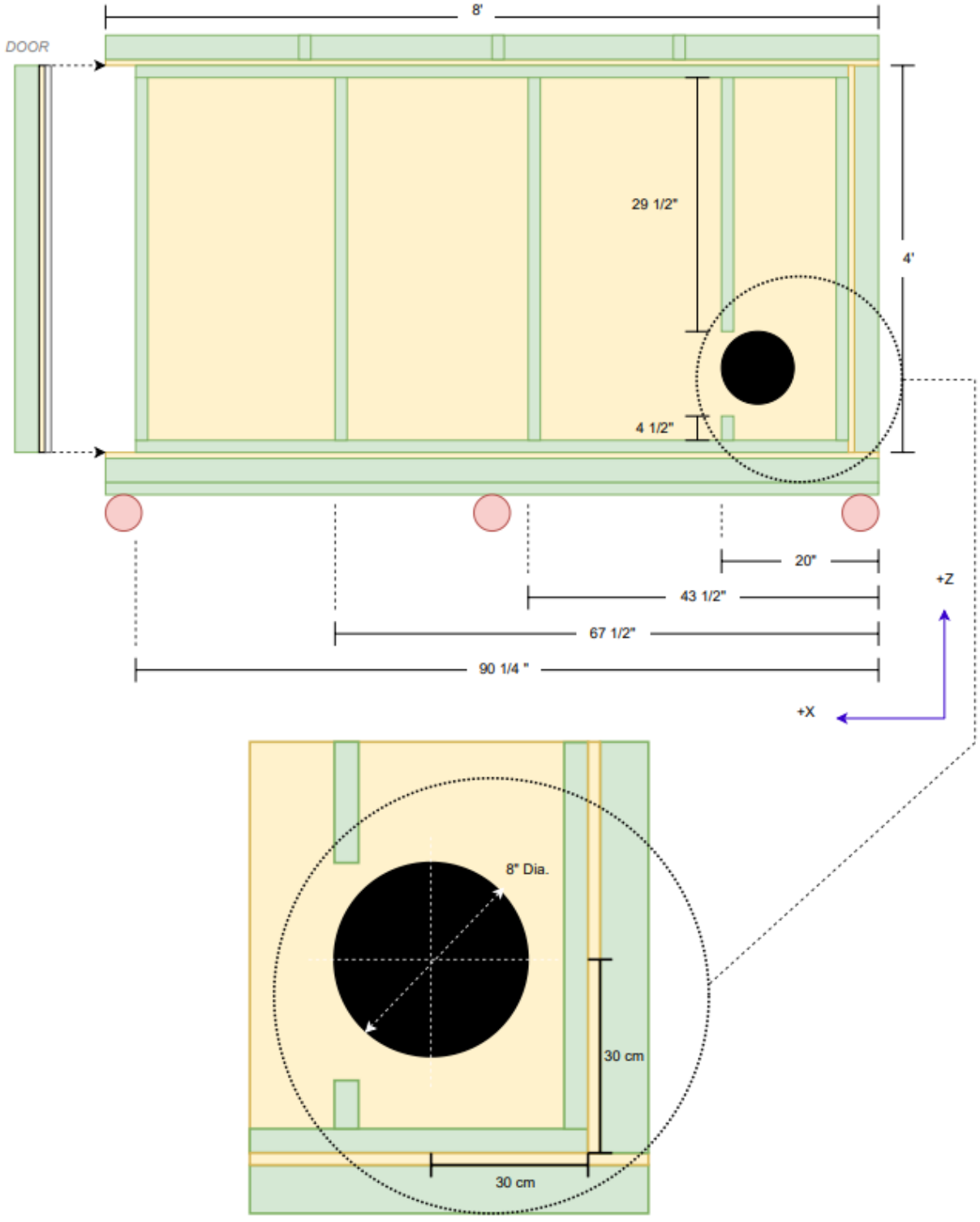

Wooden Structure (Bottom View): NOTE: Dimensions are to center of stud and extent of sheet material unless otherwise noted

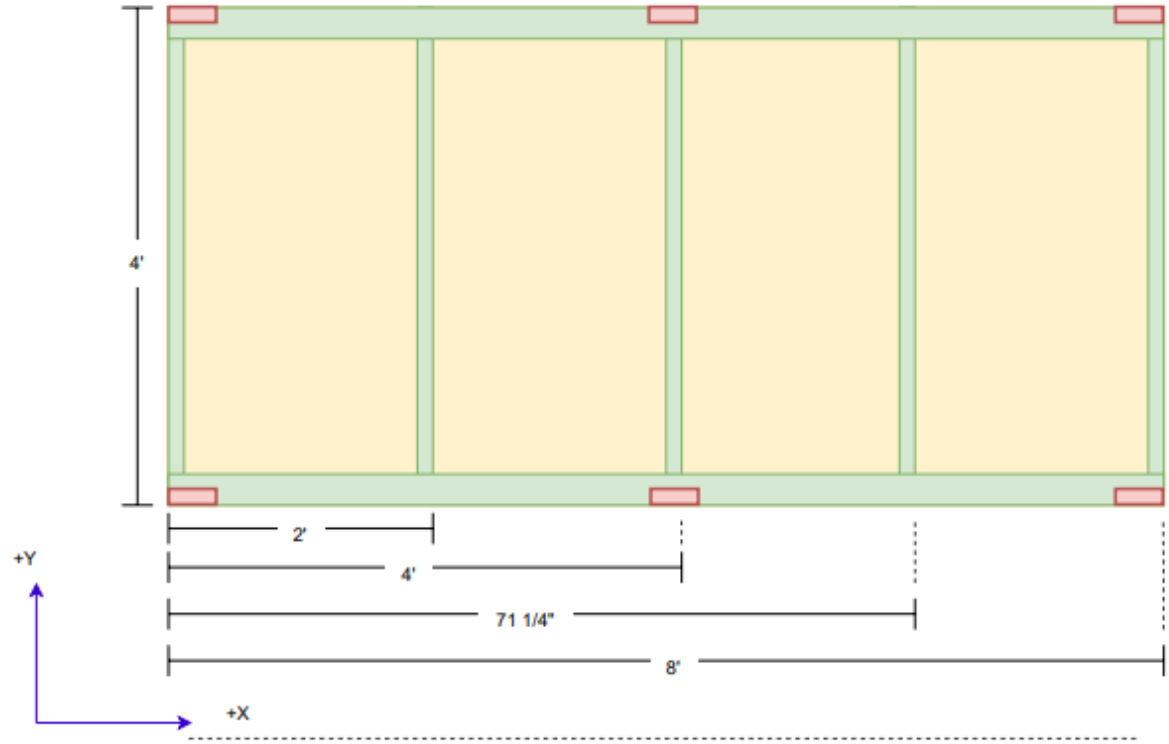

Wooden Structure (Front with Door and Back View):

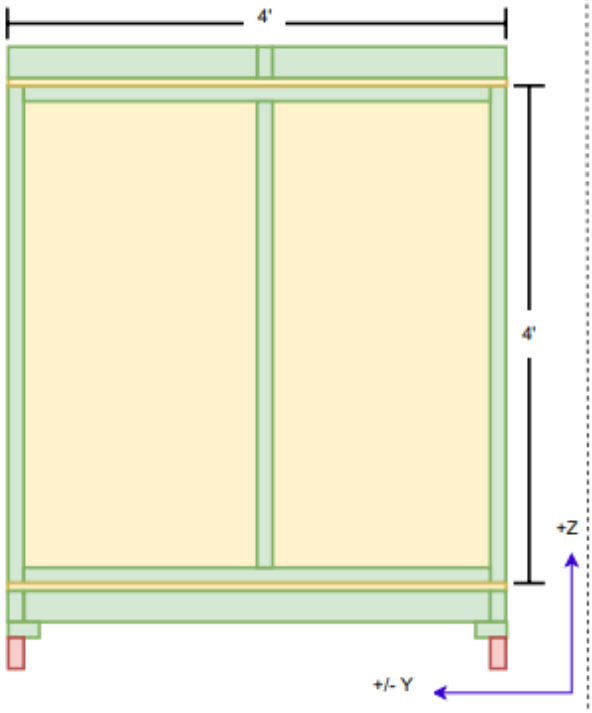

Wooden Structure (Front without door):

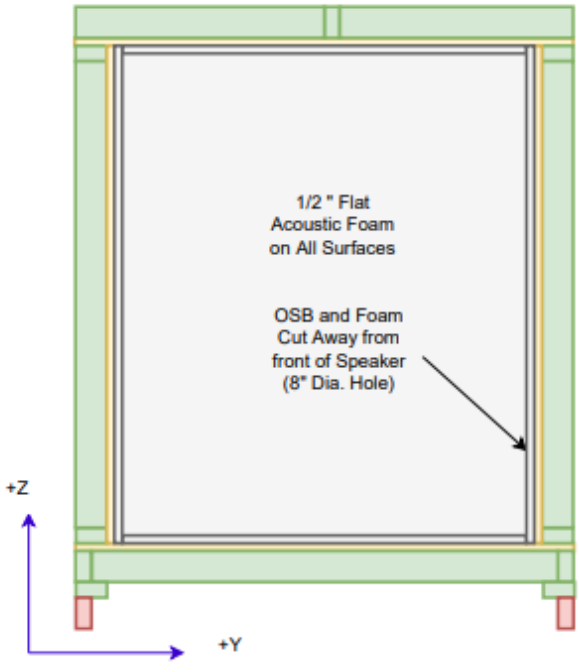

Appendix F: Acoustic Foam Mechanical/Acoustic Properties

Resources obtained from acoustic foam supplier detailing various mechanical and acoustic properties. This material is used to treat all interior faces of the enclosure [19] [20].

Property	Test Method	Values
Density (LB/Cubic Ft.)	ASTM D 3574	1.2
25% ILD (LB)	ASTM D 3574	45
Support Factor (65%/25% Min.)	ASTM D 3574	1.90
Tensile (PSI) Min.	ASTM D 3574	13.0
Elongation (%) Min.	ASTM D 3574	200
Tear (PPI) Min.	ASTM D 3574	1.30
Resiliency (%) Min.	ASTM D 3574	35
Fire Retardant Classification	CA TB #117 ASTM E84	Pass Class A (Self Extinguishing)
Contains Fire Retardant Additives	- - -	Yes Contains NO PBDEs

SOUND ABSORPTION REPORT
RAL-A11-151

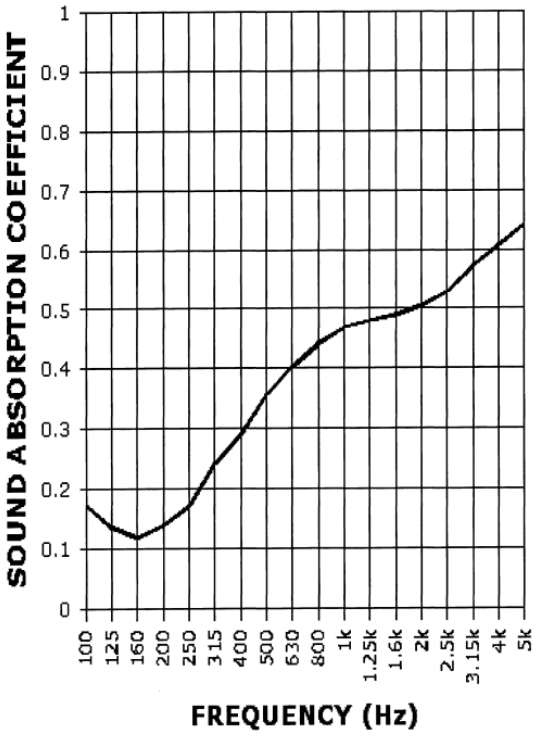

1/3 Octave Center Frequency (Hz)	Absorption Coefficient	Total Absorption In Sabins
100	0.17	12.46
** 125	0.14	9.73
160	0.12	8.46
200	0.14	9.84
** 250	0.17	12.18
315	0.24	17.35
400	0.29	20.80
** 500	0.36	25.61
630	0.40	28.95
800	0.44	31.68
** 1000	0.47	33.74
1250	0.48	34.54
1600	0.49	35.16
** 2000	0.51	36.41
2500	0.53	38.04
3150	0.57	41.19
** 4000	0.61	43.64
5000	0.64	46.29

SAA = 0.38
NRC = 0.40

References

[1] P. A. Nelson, A. D. Curtis, S. J. Elliott and A. Bullmore, "The active minimization of harmonic enclosed sound fileds, Part I: theory," *Journal of Sound and Vibration,* vol. 117, no. 1, pp. 1-13, 1987.

[2] A. J. Bullmore, P. A. Nelson, A. D. Curtis and S. J. Elliott, "The active minimization of harmonic enclosed sound fields, Part II: computer simulation," *Journal of Sound and Vibration,* vol. 117, no. 1, pp. 15-33, 1987.

[3] S. J. Elliott, A. D. Curtis, A. J. Bullmore and P. A. Nelson, "The active minimization of harmonic enclosed sound fileds, Part III: experimental verification," *Journal of Sound and Vibration,* vol. 117, no. 1, pp. 35-58, 1987.

[4] D. A. Stanef, C. H. Hansen and R. C. Morgans, "Active control analysis fo mining vehicle cabin noise using finite element modelling," *Journal of Sound and Vibration,* vol. 277, pp. 277-297, 2004.

[5] A. Ohadi and A. Emadi, "Active Noise Control Simulation in a Passenger Car Cabin Using Finite Element Modeling," *SAE Technical Paper,* 2005.

[6] A. J. Khatokar, S. Mohamady and A. Montazeri, "A Simulation Environment to Evaluate the Effect of Secondary Source Coupling for Noise Reduction in an Automotive Application," in *Proceedings from the 2022 International Conference on Automotive Audio*, Dearborn, 2022.

[7] H. Zhang and D. Wang, "Deep ANC: A deep learning approach to active noise control," *Neural Networks,* vol. 141, pp. 1-10, 2021.

[8] Science Learning Hub, "Sound - wave interference," The University of Waikato Te Whare Wananga o Waikato, 13 September 2019. [Online]. Available: https://www.sciencelearn.org.nz/resources/2816-sound-wave-interference. [Accessed 14 March 2023].

[9] S. M. Kuo and D. R. Morgan, "Active noise control: a tutorial review," *Proceedings of the IEEE,* pp. 943-973, June 1999.

[10] S. Donders, L. Hermans, E. Nauwelaerts and S. Chojin, "CAE technologies for efficient vibro-Acoustic vehicle design modification and optimization," in *Proceedings from the 23rd International Conference on Noise and Vibration Engineering*, 2008.

[11] A. Farina, "Simultaneous Measurement of Impulse Response and Distortion with a Swept-Sine Technique," in *Proceedings from the 108th AES Convention*, Paris, 2000.

[12] F. Malbos, M. K. Bogdanski and M. Strauss, "Advanced Loudspeaker Calculator - an Example of COMSOL Apps Utilization," in *The Proceedings of the 2018 COMSOL Conference*, Lausanne, 2018.

[13] A. Farina, "Advancements in impulse response measurements by sine sweeps," in *Proceedings from the 122nd AES Convention*, Vienna, 2007.

[14] HARMAN Int., "Harman Acoustic Test Data," Juarez, 2016.

[15] S. J. Elliott, P. Joseph, A. J. Bullmore and P. A. Nelson, "Active cancellation at a point in a pure tone diffuse sound field," *Journal of Sound and Vibration,* vol. 120, no. 1, pp. 183-189, 1988.

[16] T. J. Sutton, S. J. Elliott, A. M. McDonald and T. J. Saunders, "Active control of road noise inside vehicles," *Noise Control Engineering Journal,* vol. 42, no. 1, p. 137, 1994.

[17] M. Herrmann, J. Kralicek, W. Stein and F. Gauterin, "Describing Road Booming Noise with a Hybrid Simulation Model Using a Time Segmentation of the Excitation Load Approach," *Vehicles,* vol. 3, no. 3, pp. 469-479, 2021.

[18] W. Jung, S. Elliott and J. Cheer, "The effect of remote microphone technique and head-tracking on local active sound control," in *Proceedings from the 23rd International Congress on Sound & Vibration*, Athens, 2016.

[19] Foam Factory, Inc., "Acoustic Foam Datasheet," Macomb, 2014.

[20] Riverbank Acoustic Laboratories, "ASTM C423-09a and E795-05 Sound Absorption Test Report," Geneva, 2011.